

Dear Editor;

We have carefully reviewed the referee's comments and we addressed all of them. We think that we have pointed out all the issues questioned by the referee and offer an adequate discussion, brief, and kept the length of the discussion. All changes were highlighted in the text. The lines with changes and the new lines are indicated below.

We hope that this version is appropriate for publication in your prestigious journal.

Sincerely yours,
Práxedes Muñoz
On behalf of all authors

Referee suggestion:

Referee: The paragraphs in the Discussion section are extremely long, I suggest dividing the long paragraphs into two or three to facilitate the readability of the manuscript.

Answer: We separated the long paragraphs into shorter ones.

Referee: Lines 410-412: Move "We use Al as a normalizing parameter for the enrichment/depletion of elements due to its conservative behavior. The elements are presented as metal/Al ratios" the Methods section

Answer: We moved these lines to the Methods section. Lines 251-258.

Referee: Line 438: add "in core BTGC8" after "were lower"

Answer: We added this sentence in line 447.

Referee: Lines 440-446: Move the first 3 sentences to the Methods section.

Answer: These lines were moved to the Methods section. Lines 249-251

Referee: Lines 652: Yes, it seems to be contradictory, but a similar trend (trend towards higher productivity associated with decreasing reducing conditions) was observed off Peru (Salvatteci et al., 2014; Cardich et al., 2019). These authors based their observations on d15N, redox sensitive metals and benthic foraminifera assemblages. I suggest citing these papers and discuss whether the mechanisms proposed by these authors can explain or not the observed pattern off Guanaqueros Bay (BGGC5) and Tongoy Bay (BTGC8).

Answer: We considered the referee's suggestion and we added other references to discuss the main mechanisms proposed for this oxygenation at coastal areas. Lines 662-677

Referee: Lines 693-696. The westerlies were located in a more poleward position during the mid-Holocene (Lamy et al. 2001). Mollier-Vogel et al. (2019) erroneously indicate, citing Lamy et al. (2001), that during the mid-Holocene the Westerlies were situated in a more northward position (see Salvatteci et al., 2019, for further discussion on this topic). This needs

to be corrected in the manuscript and the original citation must be also included (Lamy et al., 2001).

Answer: We modified the paragraph changing the reference indicated by the referee. Lines 724-734

Referee: Lines 725-730. The authors need to briefly compare and contrast their results with the reconstructed shifts of the storm tracks of the westerlies (Lamy et al., 2001).

Answer: We discussed the southern Westerlies shifts in several paragraph; we compared our records in a general view for all SE Pacific first, and then reviewed the records for north-central Chile, establishing the main environmental conditions reported for the region. Lines 735-746, lines 778-780.

Referee: Lines 763-767. Mollier et al. (2019) show evidence for decreased denitrification during the Mid-Holocene based on multiple $d^{15}N$ records along the coast. They do not show evidence for changes in sediment redox conditions. Rephrase this sentence or provide a better reference.

Answer: A decreased denitrification implies a change in the redox condition and an oxygenation of the bottoms. Therefore, the reference is appropriate. We added a sentence for further clarity. Lines 811-812

1 **Reconstructing past variations in environmental conditions and paleoproductivity**
2 **over the last ~8000 years off north-central Chile (30° S)**

3
4 Práxedes Muñoz^{1,2}, Lorena Rebolledo^{3,4}, Laurent Dezileau⁵, Antonio Maldonado^{2,6},
5 Christoph Mayr^{7,8}, Paola Cárdenas^{5,9}, Carina B. Lange^{4,10,11}, Katherine Lalangui¹⁰,
6 Gloria Sanchez¹², Marco Salamanca¹⁰, Karen Araya^{1,13}, Ignacio Jara², Gabriel Vargas¹⁴,
7 Marcel Ramos^{1,2}

8
9 ¹Departamento de Biología Marina, Universidad Católica del Norte, Larrondo 1281,
10 Coquimbo, Chile.

11 ²Centro de Estudios Avanzados en Zonas Áridas (CEAZA), Coquimbo-La Serena,
12 Chile.

13 ³Departamento Científico, Instituto Antártico Chileno, Punta Arenas, Chile

14 ⁴Centro FONDAF de Investigación Dinámica de Ecosistemas Marinos de Altas
15 Latitudes (IDEAL), Universidad Austral de Chile, Campus Isla Teja, Valdivia, Chile.

16 ⁵Normandie University, UNICAEN, UNIROUEN, CNRS, M2C, 14000 Caen, France.

17 ⁶Instituto de Investigación Multidisciplinario en Ciencia y Tecnología, Universidad de
18 La Serena, La Serena, Chile.

19 ⁷Institut für Geographie, FAU Erlangen-Nürnberg, 91058 Erlangen, Germany.

20 ⁸Department of Earth and Environmental Sciences & GeoBio-Center, LMU Munich,
21 80333 Munich.

22 ⁹Programa Magister en Oceanografía, Universidad de Concepción, casilla 160C,
23 Concepción, Chile.

24 ¹⁰Departamento de Oceanografía, Facultad de Ciencias Naturales y Oceanográficas,
25 Universidad de Concepción, Casilla 160C, Concepción, Chile.

26 ¹¹Centro de Investigación Oceanográfica COPAS Sur-Austral, Universidad de
27 Concepción, Casilla 160C, Concepción, Chile.

28 ¹²Universidad de Magallanes, Punta Arenas, Chile.

29 ¹³Laboratoire Géosciences Montpellier (GM), Université de Montpellier, 34095
30 Montpellier Cedex 05, France.

31 ¹⁴Departamento de Geología, Universidad de Chile, Santiago, Chile.

32

33 *Correspondence to:* Práxedes Muñoz (praxedes@ucn.cl)

34

35 **Abstract**

36

37 The aim of this project was to establish past variations in the main oceanographic and
38 climatic features of a transitional semi-arid ecosystem in the north-central Chilean coast.
39 We analyzed recent sedimentary records retrieved from two bays, Guanaqueros and
40 Tongoy (30° S), for geochemical and biological analyses, including the following:
41 sensitive redox trace elements, biogenic opal, total organic carbon (TOC), diatoms, and
42 stable isotopes of organic carbon and nitrogen. Three remarkable periods were
43 established with different environmental conditions and productivities: (1) > cal BP
44 6600, (2) cal BP 4500–1800, and (3) cal BP 140 to the present (CE 2015). The first
45 period was characterized by a remarkably higher productivity (higher diatom
46 abundances and opal) in which large fluxes of organic compounds were also inferred
47 from the accumulation of elements, such as Ba, Ca, Ni, Cd, and P in the sediments.
48 Meanwhile, significantly reduced conditions at the bottom of the bays were suggested
49 based on the large accumulation of Mo, Re, and U, showing a peak at cal BP 6600 when
50 sulfidic conditions could have been present. According to the pollen moisture index,
51 this was also identified as the driest interval. These conditions should be associated with
52 an intensification of the Southern Pacific Subtropical Anticyclone and stronger
53 southerly western winds, emulating the La Niña-like conditions, as has been described
54 for the SE Pacific during the early Holocene and part of the mid-Holocene. During most
55 of the second period, lower productivity was observed; however, a small increase was
56 identified between Cal BP 3400 and 4000, although lower amounts of diatom (valves g⁻¹)
57 and nutrient-type metal accumulations were evident. Anoxic conditions at the bottom
58 of the bays changed to an almost stable sub-oxic condition during this time interval. The
59 third period was marked by intense oxygenation after cal BP 1800, as observed by a
60 drastic change in the accumulation of U, Mo, and Re. This was followed by a return to
61 more reduced conditions over the past two centuries, characterized by a small
62 productivity rise after cal BP ~140, as suggested by the opal accumulations. Overall,
63 lower primary productivity, lower reduced conditions at the bottom, and higher
64 humidity conditions were established after cal BP 6600 to the present. We suggest that
65 the oxygenation might be associated with a weak effect from the oxygen minimum zone
66 over the shelf and intensified El Niño activity, introducing oxygenated waters to the
67 coastal zones through the propagation of equatorial waves and establishment of

68 conditions that reduced the primary productivity from the mid-Holocene toward the
69 beginning of the modern era.

70 Keywords: paleoproductivity, paleoredox, trace metals, diatoms, opal, organic carbon,
71 Coquimbo, SE Pacific

72

73 **1. Introduction**

74

75 The mean climatic conditions in the SE Pacific are modulated by the dynamics of the
76 Southern Pacific Subtropical Anticyclone (SPSA) and Humboldt Current System. The
77 coastal wind pattern produced alongshore varies along the SE Pacific, showing lower
78 seasonality between 18°–30° S and producing semi-permanent upwelling (Pizarro et al.,
79 1994; Figueroa and Moffat, 2000). This system is highly affected by the inter-annual
80 variability imposed by the El Niño Southern Oscillation (ENSO), impacting the wind
81 intensity and, therefore, the productivity (Rutland and Fuenzalida, 1991; Blanco et al.,
82 2002). Other climate patterns demonstrate impacts at longer timescales (inter-annual,
83 decadal, inter-decadal), such as the Pacific Decadal Oscillation (PDO) and the Southern
84 Annular Mode (SAM). These patterns modify the strength and position of the southerly
85 western winds (SWW), producing cold/warm periods that affect mainly winter
86 precipitation during the positive/negative trends of the SAM and lead to intense/weak
87 upwelling (Quintana and Aceituno, 2012; Ancapichún and Garcés-Vargas, 2015). In
88 addition, the orbitally induced variations in the austral insolation influences the extent
89 of the Antarctic sea ice and the Hadley cell, which act as important forces in the
90 latitudinal displacement of the Inter-tropical Convergence Zone (ITCZ; Kaiser et al.,
91 2008, and references therein). These fluctuations produce humid and arid conditions
92 along the SE Pacific where the intensity of the wind remains the key factor in the
93 upwelling strength and, therefore, the supply of nutrients to the photic zone, all of which
94 are required for the development of the primary productivity.

95 Off Coquimbo (30° S), there is normally semi-permanent and intense upwelling forced
96 by local winds, strongly influenced by topographic features (Figueroa and Moffat,
97 2000) and ENSO variability (Schaffer et al., 1997; Escribano et al., 2004). During El
98 Niño, the intensities of the mean winds alongshore are reduced (conversely, during La
99 Niña) (Rahn and Garreaud, 2013), impacting the upper circulation of the ocean and
100 affecting the oxygenation of the water column and strength of the upwelling. The high
101 productivity that takes place close to the coast during normal periods (Escribano et al.,

102 2004 and references therein) maintains a zone of low dissolved oxygen content,
103 reinforcing the oxygen minimum zone (OMZ; Helly and Levin, 2004, Ulloa et al.,
104 2012); however, the opposite occurs during El Niño, in which oxygenated waters enter
105 the coastal zone provided by the narrow continental shelf (Helly and Levin, 2004). This
106 changes the normal suboxic conditions at the bottom, normal composition of
107 macrofauna, and related geochemical characteristics of the sediments, with implications
108 that persist for several years after the event (Gutiérrez et al., 2006; Sellanes et al., 2007).
109 These changes in primary productivity and oxygenation at the bottom can be observed
110 in the sedimentary records that respond to the amount of organic carbon that has settled
111 on the surface sediments under different oceanographic and climatic conditions. The
112 diagenetic reactions during organic matter remineralization produce the enrichment or
113 depletion of trace elements, which reflects the amount of settled organic matter but also
114 reinforces the low oxygen conditions imposed by the OMZ, all of which promotes the
115 enrichment or depletion of trace elements (Tribovillard, 2006). Their variability in
116 sedimentary records has been extensively used to establish temporary changes in
117 primary productivity and changes in the oxygenation at the bottom (Nameroff et al.,
118 2002; Zheng et al., 2002; McManus et al., 2006; Siebert et al., 2003).
119 North-central Chile is a semi-arid zone that does not receive large fluvial contributions,
120 except during abnormal periods such as in El Niño years, during which higher runoff
121 has been recorded in austral winter (Valle-204; Levinson et al., 2000; Montecinos and
122 Aceituno, 2003; Garreaud et al., 2009). Under this scenario, marine sediments are often
123 highly influenced by primary production in the water column and terrestrial runoff;
124 therefore, sedimentary records can reveal the past variability in primary production and
125 oceanographic conditions over the shelf, which ultimately respond to the major
126 atmospheric patterns in the region. We considered that redox trace elements off
127 Coquimbo (30° S) respond to changes in the local hypoxia (U, Mo, and Re); in addition,
128 the nutrient-type elements are assumed to have followed the organic flux variability of
129 the sediments (Ba, Ni Cu), according to the interannual and interdecadal variability
130 described for the climatic and oceanographic settings in the region. Similarly, we
131 measured Ca, K, and Pb to assess the terrigenous inputs from runoff and aeolian
132 transportation, which is also impacted by Fe and Mn (Calvert and Pedersen, 2007). Ca
133 accumulation depends, in turn, on carbonate productivity and dissolution, and has also
134 been used as a paleoproductivity proxy (Paytan, 2008; Govin et al., 2012). We
135 determined the enrichment/depletion of elements to establish the primary prevailing

136 environmental conditions during the sedimentation of particulate matter (Böning et al.,
137 2009). In addition, we considered the diatom assemblages with biogenic opal as a
138 measurement of siliceous export production, total organic carbon (TOC), and stable
139 isotopes to identify variations in the organic fluxes to the bottom. Moreover, pollen
140 grains were used to identify environmental conditions based on the climate relationship
141 of the main vegetation formations in north-central Chile. Based on our records we were
142 able to identify wet/dry intervals, periods with high/low organic fluxes to the sediments,
143 which are related to changes in primary production, and changes in the redox conditions
144 at the bottom, which in turn, have been associated with the main climatic conditions
145 described for the Holocene in this region.

146

147 **2. Study area**

148 The Coquimbo area (29–30 °S), in the southern limit of the north-central Chilean
149 continental margin, constitutes a border area between the most arid zones of northern
150 Chile (Atacama Desert) and the more mesic Mediterranean climate in central Chile
151 (Montecinos et al., 2016). Here, the shelf is narrow, and several small bays trace the
152 coast line.

153 The Tongoy and Guanaqueros bays are located in the southern edge of a broad
154 embayment between small islands to the north (29 °S; Choros, Damas, and Chañaral)
155 and Lengua de Vaca Point to the south (30 °S) (Fig. 1), protected from southerly winds
156 that are predominant in the region. Tongoy Bay is a narrow marine basin (10 km at its
157 maximum width) with a maximum depth of approximately 100 m. To the northeast lies
158 Guanaqueros Bay, a smaller and shallower basin. High wind events are evenly
159 distributed throughout the year and promote an important upwelling center at Lengua de
160 Vaca Point, resulting in the accumulation of high biomass along a narrow coastal area
161 (Moraga-Opazo et al., 2011; Rahn and Garreaud, 2013) that reach concentrations of
162 approximately 20 mg m⁻³ (Torres and Ampuero, 2009). In the shallow waters of Tongoy
163 Bay, the high primary productivity results in high TOC in the water column, allowing
164 for the deposition of fine material to the bottom; TOC rises concurrently with periods of
165 low oxygen (Fig. 2; Muñoz et al., unpublished data). Recent oceanographic studies
166 indicate that low dissolved oxygen water intrusions from the shelf (Fig. 3) seem to be
167 related to lower sea levels, resulting from annual local wind cycles at a regional meso-
168 scale (Gallardo et al., 2017). Oceanographic time series indicate that transition times
169 develop in short periods due to changes in the direction and intensity of the winds along

170 the coast, with strong seasonality (<http://www.cdom.cl/boyas-oceanograficas/boya->
171 tongoy). The spatial and temporal variability of these processes is still under study. In
172 addition, oceanic variability along the western coast of South America is influenced by
173 equatorial Kelvin waves on a variety of timescales, from intra-seasonal (Shaffer et al.,
174 1997) and seasonal (Pizarro et al., 2002; Ramos et al., 2006), to inter-annual (Pizarro et
175 al., 2002; Ramos et al., 2008).

176 Sedimentological studies are scarce with regard to the north-central shelf of Chile. A
177 few technical reports indicate that sediments between 27° S and 30° S are composed of
178 very fine sand and silt with relatively low organic carbon content (< 3 and ~5%), except
179 in very limited coastal areas where organic material accounts for approximately 16% of
180 the total material (Muñoz, unpublished data; FIP2005-61 Report, www.fip.cl). Coastal
181 weathering is the main source of continental input owing to scarce river flows and little
182 rainfall in the zone (0.5–80 mm y⁻¹; Montecinos et al., 2016, Fig. 1). Freshwater
183 discharges are represented by creeks, which receive the drainage of the coastal range
184 forming wetland areas in the coast and even small estuaries, such as Pachingo, located
185 south of Tongoy (Fig. 1). These basins cover ~300 and 487 km², respectively. The water
186 volume in the estuaries is maintained by the influx of seawater mixed with the
187 groundwater supply. Normally, a surface flux to the sea is observed. Freshwater
188 discharges only occur through dry creeks that drain water during high rainfall periods in
189 the coastal zone (Dirección General de Aguas, 2011).

190

191 **3. Materials and methods**

192 **3.1. Sampling**

193 Sediment cores were retrieved from two bays in the Coquimbo region: Bahía
194 Guanaqueros (core BGGC5; 30° 09' S, 71° 26' W; 89 m water depth) and Bahía Tongoy
195 (core BTGC8; 30° 14' S, 71° 36' W; 85 m water depth) (Fig. 1), using a gravity corer
196 (KC-Denmark) during May 2015, onboard the L/C Stella Maris II owned by the
197 Universidad Católica del Norte. The length of the cores was 126 cm for BGGC5 and 98
198 cm for BTGC8.

199 Subsequently, the cores were sliced into 1 cm sections, and subsamples were separated
200 for grain size measurements and determination of magnetic susceptibility, trace element
201 and biogenic opal concentrations, C and N stable isotope signatures ($\delta^{13}\text{C}$, $\delta^{15}\text{N}$), and
202 TOC content. The samples first were kept frozen (–20° C) and then freeze-dried before
203 laboratory analyses.

204

205 **3.2. Geochronology (^{210}Pb and ^{14}C)**

206 A geochronology was established combining ages estimated from $^{210}\text{Pb}_{\text{xs}}$ activities
207 suitable for the last 200 years and radiocarbon measurements at selected depths for
208 older ages. The quantification of ^{210}Pb activities was performed through the alpha
209 spectrometry of its daughter ^{210}Po following the procedure of Flynn (1968). The
210 (unsupported) activities of $^{210}\text{Pb}_{\text{xs}}$ were determined as the difference between the ^{210}Pb
211 and ^{226}Ra activities measured in some intervals of the sediment column. Meanwhile,
212 ^{226}Ra was measured by gamma spectrometry at the Laboratoire Géosciences of the
213 Université de Montpellier (France). Standard deviations (SD) of the ^{210}Pb inventories
214 were estimated by propagation of the counting uncertainties (Bevington and Robinson,
215 1992) (Table S1, supplementary data). The ages were based on the Constant Rate of
216 Supply Model (CRS, Appleby and Oldfield, 1978).

217 Radiocarbon measurements were performed on a mix of planktonic foraminifer species
218 in core BGGC5, whereas the benthic foraminifer species *Bolivina plicata* was selected
219 for core BTGC8 (Table 1). The samples were submitted to the National Ocean Sciences
220 AMS Facility (NOSAMS) of the Woods Hole Oceanographic Institution (WHOI). The
221 timescale was obtained from $^{210}\text{Pb}_{\text{xs}}$ and ^{14}C measurements and from Bacon age–depth
222 modeling open source software (Blaauw and Christen, 2011), considering the Marine
223 curve ^{13}C (Reimer et al., 2013) (Fig. 4) and a reservoir deviation from the global mean
224 reservoir age of 441 ± 35 y. This was estimated subtracting the ^{14}C age value
225 corresponding at the historical dates 1828 AD and 1908 AD (499 ± 24 and 448 ± 23 ^{14}C
226 y, respectively, Reimer et al., 2013) from the apparent ^{14}C age of the foraminifers
227 measured at depths of 5 and 10 cm for cores BTGC8 and BGGC5, respectively
228 (Sabatier et al., 2010; Table 2).

229

230 **3.3. Geophysical characterization**

231 The magnetic susceptibility ($\text{SI} \times 10^{-8}$) was measured with a Bartington Susceptibility
232 Meter MS2E surface scanning sensor at the Sedimentology Laboratory at Centro Eula,
233 Universidad de Concepción. Mean values from three measurements were calculated for
234 each sample.

235 The grain size was determined using a Mastersizer 2000 laser particle analyzer (Hydro
236 2000–G, Malvern) in the Sedimentology Laboratory at Universidad de Chile. Skewness,

237 sorting, and kurtosis were evaluated using the GRADISTAT statistical software (Blott
238 and Pye, 2001), which includes all particle size spectra.

239

240 3.4. Chemical analysis

241 Trace element analyses were performed via inductively coupled plasma-mass
242 spectrometry (ICP-MS) using an Agilent 7700x at Université de Montpellier (OSU
243 OREME/AETE regional facilities). The analysis considered reference materials (UBN,
244 BEN, and MAG1) that had an accuracy higher than $\pm 5\%$; the analytical precisions were
245 between 1% and 3%. Internal standardizations with In and Bi were used to deconvolve
246 the mass-dependent sensitivity variations of both matrix and instrumental origin
247 occurring during the course of an analytical session. The analytical precisions attained
248 were between 1% and 3%.

249 The element concentrations were normalized using Al due to its conservative behavior
250 that allows assessing the relative enrichment/depletion of elements and evaluating the
251 crustal contribution for each element (Calvert and Pedersen, 2007). The authigenic
252 enrichment factor (EF) was estimated as: $EF = (Me/Al)_{\text{sample}} / (Me/Al)_{\text{detrital}}$, where
253 $(Me/Al)_{\text{sample}}$ is the bulk sample metal (Me) concentration normalized to the Al content,
254 and the denomination “detrital” indicates a lithogenic background (Böning et al., 2009).
255 Detrital ($[Me]_{\text{detrital}}$ and $[Al]_{\text{detrital}}$) concentrations were established considering the local
256 metal abundance, which is more accurate than using mean Earth crust values (Van der
257 Weijden, 2002). We used average element concentrations on surface sediments (0–3
258 cm) of the Pachingo wetland (Table 3).

259 TOC and stable isotope ($\delta^{15}\text{N}$ and $\delta^{13}\text{C}$) analyses were performed at the Institut für
260 Geographie, Friedrich Alexander Universität (FAU) Erlangen-Nürnberg, Germany
261 using a Carlo Erba elemental analyzer NC2500 and an isotope-ratio-mass spectrometer
262 (Delta Plus, Thermo-Finnigan) for isotopic analysis. Stable isotope ratios were reported
263 in the δ notation as the deviation relative to international standards (Vienna Pee Dee
264 Belemnite for $\delta^{13}\text{C}$ and atmospheric N_2 for $\delta^{15}\text{N}$); thus, $\delta^{13}\text{C}$ or $\delta^{15}\text{N} = [(R \text{ sample}/R$
265 $\text{standard}) - 1] \times 10^3$, where R is $^{13}\text{C}/^{12}\text{C}$ or $^{15}\text{N}/^{14}\text{N}$, respectively. The typical precision
266 of the analyses was $\pm 0.1\%$ for $\delta^{15}\text{N}$ and $\delta^{13}\text{C}$.

267 Biogenic opal was estimated following the procedure described by Mortlock and
268 Froelich (1989). The analysis was performed by molybdate-blue spectrophotometry
269 (Hansen and Koroleff, 1999), conducted at the laboratories of Marine Organic

Comentario [A1]: This paragraph was moved from the result section (4.4. Trace elements distribution, line 440) to methods section, according reviewer suggestion.

270 Geochemistry and Paleoceanography, University of Concepción, Chile. Values for
271 biogenic opal were expressed by multiplying the Si (%) by 2.4 (Mortlock and Froelich,
272 1989). The analytical precision was $\pm 0.5\%$. Accumulation rates were determined based
273 on the sediment mass accumulation rates and amount of opal for each core section in %.

274

275 **3.5. Microfossils analyses**

276 Qualitative abundances of siliceous microfossils were determined for every 1 cm
277 following the Ocean Drilling Program (ODP) protocol, described by Mazzullo and
278 Graham (1988). This information was used to select sections every 4, 8, and 12 cm for
279 BGGC5 and every 6 cm for BTGC8, to determine quantitative abundances of
280 microfossils (diatoms, silicoflagellates, sponge spicules, crysophytes, and phytoliths).
281 Roughly 0.5 g of freeze-dried sediment was treated according to Schrader and Gersonde
282 (1978) for siliceous microfossils. They were identified and counted under an Olympus
283 CX31 microscope with phase contrast, in which 1/5 of the slides were counted at 400X
284 for siliceous microfossils and one transect at 1000X was counted for *Chaetoceros*
285 resting spores (*Ch. RS*). Two slides per sample were counted with an estimated
286 counting error of 15%. Total diatom abundances are given in valves g^{-1} of dry
287 sediments.

288 Pollen analysis was conducted following the standard pollen extraction methodology
289 (Faegri and Iversen, 1989). The identification was conducted under a stereomicroscope,
290 with the assistance of the Heusser (1973) pollen catalog. A total of 100–250 terrestrial
291 pollen grains were counted in each sample. The pollen percentage for each taxon was
292 calculated from the total sum of terrestrial pollen (excluding aquatic taxa and fern
293 spores). Pollen percentage diagrams and zonation were generated using the Tilia
294 software (Grimm, 1987).

295 We further summarize pollen-based precipitation trends by calculating a pollen moisture
296 index (PMI), which is defined as the normalized ratio between Euphorbiaceae (wet
297 coastal scrubland) and Chenopodiaceae (arid scrubland). Thus, a positive (negative)
298 value for this index point corresponds to relatively wetter (drier) conditions.

299

300 **4. Results**

301 **4.1. Geochronology**

302 The activity of $^{210}Pb_{xs}$ (unsupported) was obtained from the surface to a depth of 8 cm
303 in the two cores, with an age of ~AD 1860 at 8 cm in both (Table S1). Greater surface

304 activities were obtained for core BGGC5 (13.48 ± 0.41 dpm g⁻¹) than core BTGC8 (5.80
305 ± 0.19 dpm g⁻¹), showing an exponential decay with depth (Fig. 4). A recent
306 sedimentation rate of 0.11 ± 0.01 cm y⁻¹ was estimated.

307 The age–depth model provided a maximum age of cal BP 7990 for core BGGC5 and cal
308 BP 8012 for core BTGC8 (Fig. 4). A mean sedimentation rate of 0.026 ± 0.012 cm y⁻¹
309 was estimated for core BGGC5, with a period of relatively low values (< 0.01 cm y⁻¹)
310 between cal BP 240 and 1500 and between cal BP ~5000 and 6400. This variation in the
311 accumulation rates occurred over a few centimeters (5 and 7 cm, respectively); thus, this
312 rapid decrease was considered as a hiatus in the age–depth modeling. The model
313 estimates the accumulation rates before and after the hiatus not auto-correlated,
314 obtaining variable sedimentation rates which are more accurate to the sedimentation
315 process. We could not resolve the length and time of hiatuses; we assumed an elapsed-
316 time of 1400 years based on the difference between the radiocarbon ages before and
317 after the hiatus and a mid-depth corresponding to those gaps. Although we did not have
318 stratigraphic evidence of these discontinuities in the sediment core, we believe that the
319 assumptions considered allowed the development of reasonable age–depth models.

320 Nevertheless, the interpretations of the proxy records were taken with caution in these
321 age ranges. For BTGC8, mean sedimentation rates were less variable in the entire core
322 at 0.013 ± 0.006 cm y⁻¹. The local reservoir deviation values were close to the global
323 marine reservoir (Table 2) and higher than other estimations along the Chilean margin
324 at shallower depths (146 ± 25 years at < 30 m water depth; Carré et al., 2016; Merino-
325 Campos et al., 2018). Our coring sites are deeper (~90 m water depth) and influenced by
326 upwelling water from Lengua de Vaca Point, which could explain such differences.

327 However, moderate differences were observed between the models using both reservoir
328 values. Thus, our estimations were based on two pre-bomb values established with ²¹⁰Pb
329 measured in sediments and ¹⁴C in foraminifers, used for the age modeling.

330

331 **4.2. Geophysical characterization**

332 Sediments retrieved from the bays showed fine grains within the range of very fine sand
333 to silt in the southern areas. There, grain size distribution was mainly unimodal, very
334 leptokurtic, more sorted, and skewed to fine grain when compared with sediments from
335 the northern areas. Sediment cores obtained from the northern areas were sandy (coarse
336 sand and gravel) with abundant calcareous debris. Longer cores of soft sediment were
337 retrieved at the southernmost areas (BGGC5 and BTGC8, Fig. 1), where the silty

338 component varied between 40% and 60% (Figs. 5a, 5b). The clay component was very
339 low at both cores (< 2%). The sediment's color ranged from very dark grayish brown to
340 dark olive brown (2.5Y 3/3–3/2) in Guanaqueros Bay (BGGC5) and from dark olive
341 gray to olive gray (5Y 3/2–4/2) in Tongoy Bay (BTGC8). Visible macro-remains (snails
342 and fish vertebrae) were found, as well as weak laminations at both cores. The magnetic
343 susceptibility showed higher values close to the surface, up to 127×10^{-8} SI at BGGC5,
344 and lower values (85×10^{-8} SI) at BTGC8. At greater depths, however, the values were
345 very constant, at $5\text{--}8 \times 10^{-8}$ SI at BGGC5 core and $12\text{--}20 \times 10^{-8}$ SI at BTGC8 core. In
346 both cores, susceptibility rose substantially in the last century (Figs. 5a, 5b). Lower bulk
347 densities were estimated at core BGGC5 ($0.7\text{--}0.9 \text{ g cm}^{-3}$), compared with core BTGC8
348 ($> 1 \text{ g cm}^{-3}$) (Figs. 5a, 5b). Consistent with this, the mean grain size amounted to 60–80
349 μm in Guanaqueros Bay (BTGC8), compared with 50–60 μm in Tongoy Bay
350 (BGGC5). Both cores were negatively skewed, with values of -1 to -1.2 at BGGC5,
351 and -1 to -2.5 at BTGC8. Minor increases toward coarser grain size were observed over
352 the past ~ 1000 years, especially in Tongoy Bay (BTGC8). In both cases, grain size
353 distributions were strongly leptokurtic. The Ca/Fe ratio also reduced with time, except
354 at core BTGC8 where it was only observed during the last ~ 2000 years.

355

356 **4.3. Biogenic components**

357 **4.3.1. Siliceous microfossils and biogenic opal**

358 The total diatom abundance fluctuated between 5.52×10^5 and 4.48×10^7 valves g^{-1} at
359 core BGGC5. This abundance showed good correlation with biogenic opal content at
360 BGGC5 ($R^2 = 0.52$, $P < 0.5$), with values increasing from 72 cm to the bottom of the
361 core, corresponding to cal BP 4900, and reaching their highest values before cal BP
362 6600. The opal percentage exhibited a maximum before cal BP 4900 (mode = 15.8%).
363 In contrast, the diatom abundance and biogenic opal were much lower at core BTGC8
364 ($< 2 \times 10^5$ valves g^{-1} and $< 3\%$, respectively). Here, the siliceous assemblage was almost
365 completely conformed by *Ch. RS* (Fig. 6).

366 A total of 135 and 8 diatom taxa were identified in cores BGGC5 and BTGC8,
367 respectively, whereby core BTGC8 registered very low diatom abundances. In general,
368 diatoms were the most important assemblage of siliceous microfossils (96%), followed
369 by sponge spicules (3%). The contributions of phytoliths and chrysophyte cysts was less
370 than 2% at core BGGC5. *Ch RS* was dominant in the diatom assemblage ($\sim 90\%$; Fig. 6)
371 and included the species *C. radicans*, *C. cinctus*, *C. constrictus*, *C. vanheurckii*, *C.*

372 *coronatus*, *C. diadema*, and *C. debilis*. Other recorded upwelling group species (mainly
373 at core BGGC5) were *Skeletonema japonicum* and *Thalassionema nitzschioides* var.
374 *nitzschioides* (Table S2). Other species range from 0.3% to 6% of the total assemblage.

375

376 **4.3.2. TOC and stable isotope distribution**

377 Consistent with opal and diatoms, core BGGC5 showed higher values of TOC
378 (between 2% and 5%) compared with less than ~1.5% at core BTGC8 (Figs. 5a, 5b).
379 Furthermore, $\delta^{13}\text{C}$ was slightly higher at core BTGC8 (-20‰ to -21‰) compared with
380 core BGGC5 (-21‰ to -22‰). The former also shows slightly higher values of $\delta^{15}\text{N}$
381 from the deeper sections to the surface of the core (< 7‰ to > 10‰). This increase
382 was less evident at core BGGC5, with values of ~9‰ at depth to > 10‰ at the surface
383 (Figs. 5a, 5b). The reduced TOC content was related to the slightly higher $\delta^{13}\text{C}$ values
384 (approximately -20‰) in both cores.

385

386 **4.3.3. Pollen record**

387 Initial surveys at core BTGC8 (Tongoy Bay) revealed extremely low pollen
388 abundances, which hampered further palynology work. A comprehensive pollen
389 analysis was conducted only for core BGGC5 (Guañeros Bay). The pollen record
390 of core BGGC5 consisted of 29 samples shown in Fig. 7. The record was divided into
391 five general zones following visual observations of changes in the main pollen types
392 and was also assisted by CONISS cluster analysis.

393 Zone BG-1 (cal BP 7990–7600): This zone is dominated by the herbaceous taxa
394 Chenopodiaceae, *Leucheria*-type, Asteraceae subfamily (subf.) Asteroideae, and
395 Apiaceae with overall high values for the wetland genus *Typha* spp.

396 Zone BG-2 (cal BP 7600–6700): This zone is also dominated by Chenopodiaceae,
397 *Leucheria*-type, and Asteraceae subf. Asteroideae. In addition, other non-arboreal
398 elements, such as *Ambrosia*-type, Poaceae, Brassicaceae, and *Chorizanthe* spp.,
399 increase considerably.

400 Zone BG-3 (cal BP 6700–3500): This zone is marked by a steady decline in
401 Chenopodiaceae and *Leucheria*-type and by the increase in several other herbaceous
402 elements, such as Euphorbiaceae, *Baccharis*-type, and Brassicaceae.

403 Zone BG-4 (cal BP 3500–50): This zone is mostly dominated by Ast. subf.
404 Asteroideae and is marked by a decline in Chenopodiaceae and *Leucheria*-type. Other

405 coastal taxa, such as Euphorbiaceae, *Baccharis*-type, Asteraceae subf. Chichorioideae,
406 *Quillaja saponaria*, Brassicaceae, and *Salix* spp., also increase in this zone.
407 Zone BG-5 (cal BP 50–Present): The upper portion of the record is dominated by
408 Asteraceae subf. Asteroideae and Poaceae and is marked by higher amounts of
409 Geraniaceae, Asteraceae subf. Mutisieae, Myrtaceae, and *Q. saponaria*. Additionally,
410 this zone includes introduced pollen types such as *Rumex* spp. and *Pinus* spp. The
411 latter is not shown in Fig. 7 because its abundance was minimal.
412 Overall, the most distinctive trend revealed by core BGGC-5 is a long-term decline in
413 Chenopodiaceae and higher amounts of Euphorbiaceae and Asteraceae subf.
414 Asteroideae. Along with these changes, a further increase of several other types of
415 pollen, representative of the coastal shrub land vegetation, began at approximately cal
416 BP 6700.

417

418 **4.4. Trace element distributions**

419 Trace elements are presented as metal/Al ratios in Figs. 8a and 8b for **Guanaqueros**
420 (BGGC5) and Tongoy Bays (BTGC8), respectively. The metals that are sensitive to
421 changes in the oxygen concentration (U, Re, Mo), showed an increasing metal/Al ratio
422 from the base of core BGGC5 (cal BP ~7990) up to cal BP 6600. After this peak, these
423 ratios increased slightly toward cal BP 1800, close to the beginning of the recent era,
424 followed by a sharp reduction until present. The exception to this trend was Mo, which
425 reached a maximum value up to cal BP 6600 and then reduced steadily to the present.
426 Similarly, metal ratios at core BTGC8 increase over time; however, the peak was
427 observed at cal BP ~1000 for U and Re and at cal BP 6000 for Mo, with a second
428 minor peak at cal BP 3400. Iron revealed a clear upward trend at cal BP 3500–3800
429 for core BGGC5 and a second peak between cal BP 4500 and 6500, which was not
430 clearly observed at the Tongoy core (BTGC8). Instead, core BTGC8 showed higher
431 values before cal BP 6400. In both cores, Fe increased over the past ~80 years,
432 whereas no clear trend could be established for Mn. In general, metal/Al values were
433 higher at core BGGC5.

434 A second group of elements (metal/Al ratio), including Ca, Ni, Cd, and P (related to
435 primary productivity and organic fluxes), showed a pattern similar to that of Mo/Al of
436 core BGGC5, i.e., increasing values from cal BP ~7990, reaching the highest values
437 near cal BP 6600–7000; afterwards, the values followed a constant reducing trend
438 toward the present. Otherwise, Cu/Al (a nutrient-type element) showed a different

Comentario [A2]: We modify the redaction of these lines due to the Al normalization was explained in methods section.

439 pattern, similar to the Fe/Al distribution, with a maximum value at cal BP 3500–3800
440 and a conspicuous upward trend over the past ~80 years. A third group, consisting of
441 Ba and Sr, exhibited a similar pattern but smoother, showing the maximum values
442 before cal BP 6600. At BTGC8 core, a less clear pattern was demonstrated. Ca, Ni,
443 Cd, and P ratios at core BTGC8 showed only slightly decreasing values and very low
444 peak values compared with core BGGC5; however, Ni/Al showed increasing
445 concentrations over the past 80 years, which was not observed at core BGGC5.
446 Metal/Al ratios of Ba and Sr showed no substantial variation in time. In general, all the
447 elemental concentrations were lower in core BTGC8 than in core BGGC5 and
448 presented similar long-term reduction patterns toward the present, except for Cu, Ni,
449 and Fe.

450 The authigenic enrichment expressed as EF values, suggest a large enrichment of
451 nutrient-type elements in a period prior to cal BP 6600, following the trend of the
452 Me/Al ratios, except for Ba and Fe, which did not show authigenic enrichment. The EFs
453 exhibited a sharp decrease in enrichment in recent times after cal BP 90 (Fig. 9).

454

455 5. Discussion

456 5.1. Sedimentary composition of the cores: terrestrial *versus* biogenic inputs

457 The sediments in the southern zones of the bays are a sink of fine particles transported
458 from the north and the shelf (Figs. 5a, 5b), and respond to water circulation in the
459 Guanaqueros and Coquimbo Bays (Fig. 1) with two counter-rotating gyres moving
460 counterclockwise to the north and clockwise to the south (Valle-Levinson and
461 Moraga, 2006) (Fig. 1). The differences established by the sediment composition of
462 the bays show that the sediments of Guanaqueros Bay better represent the organic
463 carbon flux to the bottom, with higher accumulation rates (mean value: $16 \text{ g m}^{-2} \text{ y}^{-1}$)
464 and higher amounts of siliceous microfossils. Furthermore, is it a better zone than
465 Tongoy for pollen identification (Figs. 5a, 6 and 7). Both areas have sediments
466 composed by winnowed particles and relatively refractory material (C/N: 9–11),
467 which has a slightly lower isotopic composition than the TOC composition in the
468 column water (–18‰, Fig. 2) and is transported by water circulating over the shelf.

469 The isotopic variations in $\delta^{13}\text{C}$ and $\delta^{15}\text{N}$ did not clearly establish differences between
470 the sediments of the two bays; however, minor differences in $\delta^{15}\text{N}$ would indicate a
471 greater influence of the upwelling nutrient supply and OMZ on the shelf, resulting in a

Comentario [A3]: These words were added according reviewer suggestion.

Comentario [A4]: Several lines were moved to the methods section (reviewer suggestion) therefore we must to modify this line.

472 $\delta^{15}\text{N}$ of 9–10‰ in the Guanaqueros Bay, values which are slightly higher than that in
473 the Tongoy Bay sediments (Figs. 5a, 5b). This isotopic composition corresponds with
474 that of NO_3^- in the upwelling waters (De Pol-Holz et al., 2007) in the range of those
475 measured at north-central Chile (~11‰; Hebbeln et al., 2000, De Pol-Holz et al.,
476 2007, 2009). This is due to the isotopic fractionation of NO_3^- during nitrate reduction
477 within the OMZ, which leaves remnant NO_3^- enriched in ^{15}N (Sigman et al., 2009;
478 Ganeshram et al., 2000 and references therein). This is particularly relevant because it
479 demonstrates the relevance of OMZ over the shelf sediments off Coquimbo at shallow
480 depths and the influence of the poleward undercurrent from the Perú OMZ (Mollier-
481 Vogel et al., 2012).

Comentario [A5]: A separate point was introduced on this line.

482 At sediment core BTGC8, lower values (< 8‰) measured at greater depths within the
483 core should account for a mix with isotopically lighter terrestrial organic matter
484 (Sweeney and Kaplan, 1980), owing to its proximity to a small permanent wetland in
485 the southern side of Tongoy Bay (Pachingo), the sediments of which have $\delta^{15}\text{N}$ of 2–
486 6‰ (Muñoz et al., data will be published elsewhere). This suggests that the Tongoy
487 sediments contain a greater proportion of continental material compared to
488 Guanaqueros Bay (Fig. 5b).

Comentario [A6]: These lines were modify for a better explanation

489 Thus, cores BGGC5 and BTGC8 in the Guanaqueros and Tongoy Bays record the
490 variability in oceanographic conditions; however, in the Tongoy core, the
491 concentration of oceanographic proxies is diluted owing to the input of terrigenous
492 material. This helps to decipher the climatic variability, considering that the main
493 input of clastic material to the area takes place during major flooding events.
494 Additionally, the main circulation of the bay system leads to favorable conditions for
495 the sedimentation and preservation of organic marine proxies in Guanaqueros Bay,
496 making the sedimentary records of these sites complementary.

497

498 **5.2. Temporal variability of primary productivity and the oxygenation of bottoms**

499 Ca, Sr, Cd, and Ni profiles suggest a lower share of organic deposition over time
500 (Figs. 8a, 8b), consistent with the slight reduction in TOC content observed in the
501 sediments (Figs. 5a, 5b) and concomitant with the other elements related to organic
502 fluxes to the bottom and primary productivity. Similarly, the maximum Ba
503 concentrations indicate higher productivity before cal BP 6600. The same is true for

504 Ca, Cd, and Ni, suggesting that the maximum productivity and organic fluxes to the
505 bottom occurred during this period. After this age, the reduction in TOC and other
506 nutrient-type elements (Ni, Sr, Ca, Cd) to the present is consistent with the increase in
507 oxygen at the bay bottom.

508 The slight rise in Ba in the last ~115 years (Fig. 8a) is a response to a less anoxic
509 environment, owing to better preservation within the sediments in less anoxic
510 environments with moderate productivity (Torres et al., 1996; Dymon et al., 1992) as
511 is the case with our study site (Gross Primary Productivity = 0.35 to 2.9 g C m⁻¹d⁻¹;
512 Daneri et al., 2000). This leads to a negative correlation with TOC (-0.59; Table 4),
513 owing to the remobilization of Ba under anoxic conditions before cal BP 6600.
514 Meanwhile, the P distribution showed a trend similar to that of TOC and the other
515 elements related to the organic fluxes to the bottom (Ni, Cd), although with a lower
516 correlation (~0.6). This is consistent with the distributions observed for U, Re, and Mo
517 at core BGGC5, which indicate that anoxic or suboxic conditions were developed
518 from cal BP 7990 to 1800 but were stronger before cal BP 6600 (Figs. 8a, 8b). After
519 this period and to the present, a remarkable reduction in their concentration suggests a
520 more oxygenated bottom environment, concurrent with lower organic fluxes to the
521 sediments. The Re profile shows the influence of suboxic waters not necessarily
522 associated with higher organic matter fluxes to the bottom. Since this element is not
523 scavenged by organic particles, its variability is directly related to oxygen changes
524 (Calvert and Pedersen, 2007, and references therein).

525 Otherwise, the accumulation of P depends on the deposition rate of organic P (dead
526 plankton, bones, and fish scales) on the bottom and is actively remineralized during
527 aerobic or anaerobic bacterial activity. P and TOC showed a declining trend toward
528 the present, suggesting a reduction in flux of organic matter over time, which was also
529 observed for Ni and Cd distributions. Alternatively, the reducing fluxes of organic
530 proxies could be explained by the higher remineralization of organic material settled at
531 the bottom due to higher oxygen availability, as shown by U, Mo, and Re distributions
532 (Figs. 8a, 8b). However, the lower $\delta^{15}\text{N}$, depending on the denitrification process, is
533 similar to that at deeper environments in the zone (De-Pol Holz et al., 2009),
534 suggesting that the influence of the reductive environment of OMZ over the shelf and
535 changes in U, Mo and Re records could depend mainly on the OMZ variability. Thus,

Comentario [A7]: A separate point was introduced on this line. The following line was modified for the reading continuity.

Comentario [A8]: These lines were modified for a better explanation.

536 the influence of the primary productivity on oxygen consumption at the bottom over
537 time would be secondary in this system, which is considered to be moderated in
538 productivity compared with upwelling centers in north and south Chile.

539 Productivity reconstructions were based on the qualitative relative abundances of
540 diatom and sponge spicules, quantitative diatom counts (valves g^{-1}), and biogenic opal
541 content only in core BGGC5, since core BTGC8 registered low valve counts ($< 1\%$ in
542 relative diatom abundance). However, in both cores, diatom assemblages were
543 represented mainly by *Ch. RS*, which are used as upwelling indicators (Abrantes 1988,
544 Vargas et al., 2004). The downcore siliceous productivity based on opal distribution
545 (Figs. 6 and 9) distinguished three main time intervals of higher productivity, which
546 coincided with the ages highlighted by the distribution of the sedimentary proxies
547 noted previously: (1) $> \text{cal BP } 6600$, (2) $\text{cal BP } 4500\text{--}1800$, and (3) $\text{cal BP } \sim 140$ to
548 recent times (CE 2015). Other periods between $\text{cal BP } 6600$ and $\text{cal BP } 4500$ and
549 between $\text{cal BP } 1800$ and $\text{cal BP } 140$ did not experience higher productivities.

550 At first period ($> \text{cal BP } 6600$), the opal accumulation rate was remarkably high,
551 amounting to $\sim 35 \pm 18 \text{ g m}^{-2} \text{ y}^{-1}$ (range: $16\text{--}119 \text{ g m}^{-2} \text{ y}^{-1}$, Fig. 9) when *Chaetoceros*
552 spores were predominant, indicating an intensification in upwelling. During this
553 period, all metal proxies suggest that primary productivity increases before $\text{cal BP } 6600$,
554 owing to the high concentrations and major enrichment of Ni, Ca, and P that
555 occurred in this period, concomitant with higher opal accumulation within the
556 sediments (Fig. 6 and 9). From these elements, Ni is the best indicator of organic
557 sinking flux related with diatom productivity in organic-rich upwelling sediments
558 (Böning et al., 2015), which helps to sustain our statement. In addition, the authigenic
559 enrichments of Cd were very high (> 100 , Fig. 9) resulting in high Cd/U ratios (> 2 ;
560 Fig. 9), indicative for anoxic conditions as this ratio could vary between 0.2 and 2,
561 from suboxic to anoxic environments (Nameroff et al., 2002). The Cd accumulation in
562 this period was higher than that reported for a highly productive zone off Concepción
563 in periods of high organic carbon accumulation in the sediments (~ 5 , Muñoz et al.,
564 2012). Additionally, the high enrichment of Mo (~ 20) indicates the prevalence of
565 anoxic conditions at the bottom in this period due to the control by sulfide
566 concentrations (Huerta-Diaz and Morse, 1992; Chaillou et al., 2002; Nameroff et al.,
567 2002; Sundby et al., 2004; Tribovillard et al., 2004). Our low U/Mo ratio (~ 0.3 , Fig. 9)
568 corroborates this assumption, as similar to those values reported today at shallower

569 anoxic zones off Perú interrupted by seasonal oxygenation (McManus et al., 2006;
570 Sholz et al., 2011, Salvattecí et al., 2016; Vergara et al., 2016). This is similar to our
571 shelf, notwithstanding the prevalence of very reduced conditions within the sediments.

Comentario [A9]: A separate point was introduced on this line. The following line was modified for the reading continuity

572 The enhanced reduced conditions, probably sulfidic, before cal BP 6600, favor the
573 accumulation of Mo and Cd over that of U, occurring in anoxic environments where
574 the chemocline is close to the water–sediment interface or above it, allowing the
575 formation of authigenic Mo that exceed the U uptake within the sediments (Algeo and
576 Tribovillard, 2009 and references therein). Re is enriched in less reduced conditions
577 than Mo, resulting in the lowest Re/Mo in this period (Fig. 9). This is congruent with
578 the environmental conditions at the bottom in zones of high productivity and intense
579 upwelling, where sulfidic conditions are developed owing to oxygen consumption in
580 the shallower zones and linked to the OMZ, as occur at northern Chilean regions,
581 where the main productivity is developed over the narrow shelf. Thus, the high
582 productivity before cal BP 6600 could result from a more intense upwelling that
583 generated permanent reduced conditions that became very anoxic at the bottom in this
584 period. Even so, the low oxygen conditions prevailed in the subsequent periods but
585 were less intense than before.

586 After cal BP 6400 until 4500 we obtained little information owing to a gap in the
587 sedimentary record, which made it difficult to visualize changes in the oxygenation
588 and productivity proxies in this interval. However, in the next period (cal BP 4500–
589 1800), we observe that the opal accumulation was lower than in the previous recorded
590 period, $12 \pm 4 \text{ g m}^2 \text{ y}^{-1}$ (range: $6\text{--}20 \text{ g m}^2 \text{ y}^{-1}$, peaking at cal BP 3400–4000; Fig. 9),
591 which is partially consistent with nutrient-type element distributions and element
592 enrichment (Fig. 8a, Fig. 9). Fe clearly shows higher values at approximately cal BP
593 3500 (Fig. 8a), which helped to boost primary productivity at this time, with a small
594 increase in diatom, measured as valves per gram and abundance (%) (Fig. 6). Other
595 elements showed less prominent accumulations (Ni, Cd, Ba, Ca, and P), pointing to a
596 lower organic matter deposition into the sediments during this period (Fig. 8a). Thus, a
597 decreasing trend in the primary productivity from cal BP 6600 is observed, which is
598 also consistent with observations off south-central Chile (36° S , Concepción shelf)
599 where lower accumulations of nutrient-type elements were also observed at cal BP
600 3600–4000 and cal BP 2600 than at cal BP 6200 (Muñoz et al., 2012).

Comentario [A10]: A separate point was introduced on this line. The following line was modified for the reading continuity

601 The low oxygen conditions within the sediments were maintained, despite the
602 downward trend in the primary productivity. This could be more related to the
603 manifestation of the OMZ close to the coast than the oxygen consumption during
604 organic matter remineralization, favoring Mo and Re accumulation until cal BP
605 1700–1800 (Fig. 8a). Lower Cd/U ratios (~1; Fig. 9) were estimated, suggesting higher
606 variations in the primary productivity but with moderate changes in the oxygen
607 conditions at the bottom. High Re/Mo and U/Mo ratios could indicate a shift toward
608 less reduced conditions but still anoxic, since U, Re, and Mo are highly enriched (6,
609 20, and 15, respectively; Fig. 9). U and Re accumulations occur in conditions that
610 exhibit less intense reduction but are not very favorable for Mo accumulation
611 (Morford et al., 2009). This could be caused by a lower C rain rate due to lower
612 productivity, producing low oxygen consumption and a less sulfidic environment
613 along the central-Chilean margin (30–36° S), which is in agreement with the lower
614 biogenic opal flux and diatom abundance after cal BP 6600 (Figs. 6, 9).

615 Slight increasing values of Re/Mo ratios until ~cal BP 3500 suggest a decreasing trend
616 in the reduced conditions, which became stronger after cal BP 1800. This time was
617 also highlighted in the sedimentary records off Concepcion shelf (36° S, Muñoz et al.,
618 2012) showing maximum enrichment of U and Cr near cal BP 1800, both indicating
619 less reduced conditions toward the present compared with previous periods. After this
620 age, no comparison could be made owing to a discontinuity in the sedimentary records
621 off Concepción. Notwithstanding, the suboxic conditions have prevailed until today at
622 Central Chile, where the oxygenation seems has been stronger off Coquimbo. It could
623 be caused by eddies related to the instabilities of the Peru Undercurrent (Vergara et al.,
624 2016), which seem to start operating more frequently from cal BP 1800 to the present.
625 After this age to cal BP 140, higher productivities were not found, and a second
626 discontinuity (cal BP 1500–240) impeded environmental reconstructions, with the
627 very low estimated sedimentation rate hindering the realization of sufficient time
628 resolution for the proxies in this interval.

629 After cal BP ~140 to recent times (CE 2015) (third period mentioned before), the
630 productivity increased substantially, deduced from the rise in opal accumulations
631 toward the present (mean opal value of $29 \pm 17 \text{ g m}^{-2} \text{ y}^{-1}$, range: $10\text{--}69 \text{ g m}^{-2} \text{ y}^{-1}$; Fig.
632 9); however, this corresponded with lower diatom abundances, which were observed
633 from cal BP 1800 to the present (range: $0.5\text{--}4.9 \times 10^6 \text{ valves g}^{-1}$; Fig. 6). This is likely

Comentario [A11]: A separate point was introduced on this line.

634 caused by the fact that only a few sections of the core in this interval were analyzed
635 for diatoms, leading to a low resolution for this measurement in the most recent
636 period. Another possibility is that the opal flux was overestimated owing to the fact
637 that the flux calculations were based on recent sedimentation rates, an estimation that
638 tends to be higher than at longer timescales (Sadler et al., 1999). However, the slight
639 increase in the Cd/U ratio, Ba and P enrichment could suggest an increase in the
640 primary productivity and organic fluxes to the bottom in more recent times (Figs. 8,
641 9). In addition, the main trend established before and after the hiatus indicates an
642 increase in the marine productivity, which would not be as high as in the first period
643 (before cal BP 6600). After cal BP 1800, there is an evident change to a less reduced
644 environment toward the present, suggesting a more oxygenated bottom environment
645 concurrent with a reduction in primary productivity, except for the last 140 years,
646 when the productivity has been more variable with a slight increasing trend.

647 Contrary to other metals, there is a conspicuous upward trend for Cu/Al, Fe/Al, and
648 Mn/Al in recent times, which is consistent with the decreasing trend of EFs of Re, U,
649 and Mo (Fig. 8a, 8b, Fig. 9); these estimations would not be influenced by the
650 sedimentation rates but rather the presence of oxygen. Otherwise, the highest
651 enrichment of Cu could suggest the presence of particulate forms and oxide formation
652 (Peacock and Sherman, 2004; Vance et al., 2008; Little et al., 2014) occurring in the
653 presence of an oxygenated environment that results in a high metal enrichment of Cu
654 ($EF_{Cu} = 4.6 \pm 0.5$, Fig. 9); however, suboxic conditions have prevailed, indicated by
655 the U/Mo ratios in the range of the reduced sediments, which are less than in the
656 sediments of the Peru shelf (Scholz et al., 2011; Salvattecchi et al., 2016). In addition,
657 the Cu enrichment coincides with the growing trend of industrialization in the area,
658 mainly the mining activity, which has been the main economic source for Coquimbo
659 region since 1890; therefore, the exposition of mineral ores and mine residues to the
660 environment by natural processes as intemperization and wind transportation deserve
661 attention.

662 We suggest that the slightly higher productivity in the last 140 years has occurred in a
663 more oxygenated environment, which seems contradictory. However, similar OMZ
664 weakening has been described off Central Peru from 1875 to 2004, caused by a
665 balance between the local productivity and the subsurface ventilation of the
666 intermediate circulation, operating at (multi)decadal to centennial scale, and hence

667 related to IPO and ENSO (Cardich et al., 2019). Current studies have shown that
668 changes in both the Peru-Chile Undercurrent (PCUC) and mesoscale eddy field
669 contribute to modulate the vertical and offshore extension of the OMZ at intra-
670 seasonal and seasonal time scales off central Chile (e.g. Vergara et al., 2016; Frenger
671 et al., 2018; Pizarro-Koch et al., 2019) and possibly at lower frequencies, modulating
672 the influence of the OMZ over the coastal zones. In addition, ENSO has been
673 identified as an important mechanism of the OMZ ventilation in the Tropical South
674 Eastern Pacific through horizontal and vertical eddy fluxes; thus, during El Niño, the
675 coastal trapped waves propagate poleward and the water column becomes oxygenated,
676 and contrarily deoxygenated during the La-Niña like conditions (Espinoza-Morriberón
677 et al., 2019 and references therein).

678 Several observations made at central Peruvian and south-central Chilean coasts
679 (12° – 36° S) reveal that the present-day wet/dry variability associated with ENSO has
680 a strong impact on the benthic communities. During El Niño, the large increase in the
681 oxygen levels change the biogeochemical processes at the bottom and its effects can
682 be observed several months after the event (Ulloa et al., 2001; Escribano et al., 2004;
683 Gutiérrez et al., 2006; 2008; Sellanes et al., 2007). Thus, the increased frequency and
684 intensity of El Niño at recent centuries would result in a mean effect, which is
685 observed as a gradual change in metal enrichment over time. This is explained by the
686 episodic oxygenation, which changes the original extent of the accumulation of
687 sensitive redox trace element through their remobilization to soluble forms (Morford
688 and Emerson, 1999; Morford et al., 2009).

689 The strong trend towards increasingly reduced conditions in the northern margin of the
690 SE Pacific (Peru and north of Chile) in the past decades has been explained by a
691 greater impact of local productivity on coastal hypoxia (Cardich et al., 2019; Díaz-
692 Ochoa et al., 2011), something that is not clearly observed in our records. Contrarily, a
693 gradual oxygenation in the north-central Chilean margin was observed, which may
694 rather respond to the deepening of the OMZ. The oxygenation/deoxygenation
695 mechanism can be the result of coastal-trapped waves, originating from the equator
696 and propagating along the coast, at different time scales and intensities. These modify
697 the stability of the regional current system and the pycnocline, and can trigger extra-
698 tropical Rossby waves (Pizarro et al., 2002; Ramos et al., 2006; 2008), contributing to

Comentario [A12]: We modify this paragraph, we are citing and discussing the references suggested by the referee and we add other papers to improve the discussion

699 the oxygen variability in coastal zones, with a major impacts on redox-sensitive
700 elements in the surface sediments.

Comentario [A13]: We re-organize these paragraph in agreement with the previous paragraph.

701

702 **5.3. Main climatic implications**

703 According to paleoenvironmental records, the past climate and oceanographic
704 variability have been interpreted mainly based on the past variability in the intensity of
705 the SWW and latitudinal position of the ITCZ (Veit et al., 1996; Hebbeln et al., 2002;
706 Lamy et al., 1999; Maldonado and Villagrán, 2002). The ITCZ movements from the
707 northernmost or southernmost latitudinal position depend on the different phases of
708 ENSO and PDO variability (Yang and Oh, 2020), as the main regulators of the climate
709 at the centennial and decadal scales. This has an impact over relevant oceanographic
710 characteristics, such as sea surface temperature (SST), upwelling, and accordingly,
711 productivity at the SE Pacific. We established marked differences in paleo-productivity
712 proxies and paleo-oxygenation in the last ~8000 years (Figs. 6, 8), indicating that high
713 marine productivity prevailed during our first period (cal BP 8000–6600), according to
714 what was established for central Chile between 10 and 5 ky owing to sustained mean La
715 Niña-like conditions associated with the cold phase of the PDO (positive phase) (De
716 Pol-Holz et al., 2006; Kaiser et al., 2008; Lamy et al., 2010), concomitantly with
717 reduced ENSO variability and a northward ITCZ displacement, which implies more
718 permanent southeast tradewinds and, hence, the upwelling of rich-nutrient cold waters
719 at eastern Pacific (Koutavas and Lynch-Stieglitz, 2004; Koutavas et al., 2006; Koutavas
720 et al., 2014).

721 Our high productivity records associated with low oxygen conditions at the bottom,
722 both reaching a maximum level at cal BP 6600, correspond to the highest productive
723 period and the most reductive environment at the bottoms over the past 8000 y. The
724 continental climate during this period has been described as being drier, with the
725 predominance of La Niña-like conditions according to the northerly position of the
726 ITCZ, which promote strong upwelling due to persistent southeast trades (Koutavas et
727 al., 2005). This climatic condition has been described for the tropical Pacific and SE
728 Pacific (Lamy et al., 2001; Carré et al., 2012; Koutavas et al 2014; Salvatecci et al.,
729 2019), indicating that La Niña-like conditions, developed at the mid-Holocene, resulted
730 of an intensification of the SPSA and the Walker circulation. These environmental
731 conditions are in agreement with the observations of our pollen records and productivity

Comentario [A14]: A separated point was inserted here.

732 proxies (PMI, Fig. 9), establishing favorable conditions for upwelling and development
733 of primary productivity along the South-East Pacific margin.

Comentario [A15]: This paragraph has been modified

734 For central Chile, the aridity conditions were limited until cal BP 5700 (Jenny et al
735 2002, Maldonado and Villagrán, 2006) or cal BP 4200 (Maldonado and Rozas, 2008;
736 Maldonado and Villagrán, 2002, 2006), characterized by reduced rainfall but intense
737 coastal humidity, which have been associated with coastal fogs that frequently occur
738 during the spring owing to a strengthening of the SPSA (Vargas et al., 2006; Garreaud
739 et al 2008; Ortega et al., 2012) and La Niña-like conditions, which explains the main
740 variability of the SPSA (Ancapichún and Garcés-Vargas, 2015). Similarly, for southern
741 Chile (41°S; Lamy et al., 2001), less humid conditions were described for a period
742 between cal BP 7700 and cal BP 4000, being stronger between cal BP 6000 and cal BP
743 5300, by a poleward position of the Southern Westerlies. All of this points to drier
744 conditions during the mid-Holocene, which was closely related to SPSA intensification
745 and the southern position of the Southern Westerlies.

Comentario [A16]: We add new lines in order to discuss our main results in the next paragraphs.

746 Consistent with this, a reduced ENSO variance during the early and mid-Holocene has
747 been suggested (Rein et al., 2005), indicating a less frequent or less intense warm
748 anomaly related to a Central Pacific (CP)-mode ENSO, which produce a moderate El
749 Niño events at the CP and strong La Niña off Peru (Carré et al., 2014, Mollier-Vogel et
750 al., 2019). This was favorable for upwelling and primary productivity development
751 along the Chilean and Peruvian margin. In addition, Braconnot et al. (2012) indicated
752 that this lower ENSO was linked to fresh water melting that counteracted the insolation
753 regime, pointing a more limited cold-dry period between 6700–7500 years ago, which
754 matches our records of maximum productivity (Figs. 6, 9) concomitantly with the
755 lowest bottom oxygen conditions and indicates a greater influence of the OMZ over the
756 shelf at the central-Chilean margin.

757 After the maximum productivity recorded, a decreasing trend occurred under warm and
758 humid climatic conditions, which would be because of an enhancement in regional
759 precipitation in the northern margin of SWW (Jenny et al., 2003; Maldonado and
760 Villagrán, 2006), consistent with the southern movement of the ITCZ, leading to wetter
761 climatic conditions in the southern tropics regions (Koutavas and Lynch-Stieglitz,
762 2004). A gradual rise in K/Ca, Fe, Al, and Pb distributions was observed in our cores
763 (Figs. 5, 9), usually considered to be an indicator of continental input by fluvial or aerial

764 transport (Calvert and Pedersen, 2007; Kaiser et al., 2008; Govin et al., 2012; Ohnemus
765 and Lam, 2015; Saito et al., 1992; Xu et al., 2015). This indicated that the precipitation
766 has been increasing through the mid- and late Holocene, except for a period of reduced
767 (or weak) ENSO activity reported between cal BP 6000 and 4000 (Koutavas and
768 Joanides, 2012; Carré et al., 2014). It is also consistent with the pollen records of central
769 Chile, which suggest an arid phase from cal BP 6200 until cal BP 4200 (Maldonado and
770 Villagrán, 2006). The lack of records between these ages in our cores (hiatus) prevented
771 the search for evidence to account for this period; consequently, no sharply contrasting
772 dry/humid periods were identified after cal BP 6600. Mostly, a gradual increase in
773 humidity and a weakening in paleo-productivity proxies after cal BP 4500 (Figs. 8, 9)
774 were observed, which would be consistent with the beginning of higher ENSO
775 variability for central-Chile after cal BP 5700 (Jenny et al., 2002, Maldonado and
776 Villagrán, 2002, 2006).

Comentario [A17]: A separated point was introduced here, and the next line was modified.

777 In general, the weakening of the SPSA results in a equatorward position of the Southern
778 Westerlies increasing the humidity conditions in Central Chile (Lamy et al., 2001), and
779 the ENSO variability increased from cal BP 5700, and stronger El Niño events would
780 begin after cal BP 4000–4500; concomitant with the high variability of latitudinal
781 displacements of the ITCZ related to the seasonality of insolation described for the
782 region at the mid- and late Holocene (Haug et al., 2001; Toth et al., 2012; Carré et al.,
783 2014). This is consistent with the occurrence of alluvial episodes in the area caused by
784 more frequent or heavier rainfall events over time, related to intensified Westerlies and
785 increased El Niño events observed from Peru to south of Chile (Lamy et al., 2001;
786 Jenny et al., 2002; 2003; Rein et al., 2005; Sandweiss et al., 2007; Ortega et al., 2012;
787 Ortega et al., 2019). A consequence is greater continental inputs, as suggested by our
788 sedimentary records in agreement with the pollen moisture index that indicated more
789 humid conditions through the mid-Holocene to the present. This was concomitant with
790 greater oxygenation at the bottom and reduced primary productivity. Nonetheless,
791 between cal BP 4500 and 3000, a slight increase in diatom abundance and opal
792 concentrations was observed, along with a slight accumulation in nutrient elements (Ni,
793 Cd, Fe, and Ca concentrations; Fig. 8). Small increases in the organic carbon flux and
794 Cd/U ratios (Fig. 5, 9) suggest that the increase in primary productivity could be
795 boosted by continental nutrients (Dezileau et al., 2004; Kaiser et al., 2008). This period
796 has been documented for the tropical east Pacific as a peak of La Niña activity (cal BP

Comentario [A18]: We add some lines in order to discuss the main findings of several papers including Lamy et al 2001.

797 3000–4000; Toth et al., 2012). This would also explain the increase in the productivity
798 proxies.

799 Despite the dominance of warm events described from the mid- to late Holocene, they
800 were not strong enough to change the suboxic conditions at the bottom in the north-
801 central Chilean margin, which varied little until cal BP 1800 (Figs. 8, 9; see U, Mo, and
802 Re). Actually, the periodicity of El Niño was similar between cal BP 5000 and cal BP
803 3000 and lower than modern times (Sandweiss et al., 2007), supporting the observation
804 of relatively low variability of the oxygen proxies in the sediments dependent on the
805 OMZ influence over the shelf. This implies that the upper limit location of the OMZ did
806 not drastically change during most of the mid- and late Holocene. Contrary to our
807 observations, the sediments at the Peruvian shelf were less reduced in the late-mid
808 Holocene than at present, which was due to a deepening in the OMZ by the increased
809 advection of waters enriched in oxygen from the Equatorial Undercurrent and the
810 shifting of the OMZ center toward the Chilean margin, leaving lower $\delta^{15}\text{N}$ values in
811 sedimentary records off Peru (Mollier-Vogel et al., 2019). Therefore, the enhanced
812 oxygenation of Peru and OMZ deepening translated into a decrease in the oxygen
813 conditions off north-central Chile. This period is followed by an increased El Niño
814 frequency that has been consistent with the intensification and frequency of flooding
815 events recorded in Peru and central Chile in the last ~2000 years (Rein et al., 2005;
816 Sandweiss et al., 2007; Jenny et al., 2002; Toth et al., 2012), which is concomitant with
817 the drastic oxygenation at the bottom observed in our records after cal BP 1800. In this
818 regard, the oxygen variation at the bottom would be related to a less intense effect of the
819 OMZs over the shelf at the central Chilean margin during the warm El Niño-like phases,
820 owing to a deepening of the oxycline (and vice versa during La Niña). These tend to be
821 associated with low productivity and, in turn, a reduction in the organic fluxes and
822 oxygen consumption during organic matter diagenesis.

823 After cal BP 1800, few records were obtained until cal BP 140, when we observed the
824 restoration of more reduced conditions, although lower than during previous periods.
825 This corresponds to the time of Peruvian upwelling shift due to the northward
826 displacement of the ITCZ to the modern position and the enhancement of the Walker
827 circulation (Gutiérrez et al., 2009), which establishes an intensification of the upwelling
828 in the eastern Pacific; consequently, an increase in the primary productivity, producing

Comentario [A19]: we add a line
indicating the main result of Mollier-Vogel.

829 high demand for oxygen during organic matter remineralization, as observed today,
830 which leads to stronger oxygen consumption in the northern part of the eastern margin.
831 Notwithstanding, the reduced conditions off Coquimbo in recent decades, are not
832 comparable to the environmental conditions of Peruvian margin, where stronger
833 deoxygenation has been developed at the bottom.

Comentario [A20]: we add these lines for a better explanation

835 6. Conclusions

836 Our results suggest that the geochemistry and sedimentary properties of the coastal
837 shelf environments in north-central Chile have changed considerably during the
838 Holocene period, suggesting two relevant changes in the redox conditions and
839 productivity, which point to a more reducing environment and higher productivity
840 around cal BP 6600. Afterwards, a less reducing environment along with decreasing
841 trends in primary productivity and increased humid conditions occurs with time. The
842 oxygenation of the surface limit of the OMZ has been proposed as the main
843 mechanism that controls the reduced conditions over the shelf and slope sediments
844 during the mid-Holocene, which mainly affected the Peruvian margin closed to the
845 OMZ edge. This led to contrasting conditions in the central-Chilean margin where the
846 most reduced conditions were observed, which was maintained with low variability
847 until cal BP 1800. After this age, the OMZ expression over the shelf was weak,
848 returning to more reduced conditions in recent times (two last centuries), similar to the
849 Peruvian margin but weaker at north-central Chile.

850 The northward shifts of the SWW belt, in addition to an increased frequency in El Niño
851 events, have been proposed as the main drivers for climatic conditions during this
852 period. These elements have introduced high variability in the primary productivity
853 during this time interval. This also impacted the accumulation of organic matter due to
854 an intensification of its remineralization, showing a decreasing trend in the buildup of
855 nutrient-type elements and organic carbon burial rates toward the present. Otherwise,
856 decreasing oxygen content at the bottom is highly influenced during El Niño events,
857 something that seems to have been operating at higher frequencies after cal BP 1800
858 and, especially after cal BP 140, when the most extreme events become more frequent.
859 Thus, the El Niño phenomenon and ITCZ latitudinal displacement have greatly
860 contributed to the climatic and oceanographic features in the eastern Pacific, linked to
861 the positive or negative phases of the PDO, which all has a relevant effect on the OMZ
862 position in the Chilean margin. Otherwise, oxygenation/deoxygenation changes can

863 result from coastal-trapped waves that can operate at different time scale and intensities,
864 and have strong effect on the stability of the regional current system and the pycnocline
865 position in the coastal zones.

Comentario [A21]: new lines added

866 Finally, these changes highlight the sensitivity of these environments to climate
867 variability at different timescales, which is consistent with the description of past
868 regional climatic trends. Based on the dramatic changes observed in the past centuries,
869 future changes are expected in the context of global warming at unprecedented rates.

870

871 7. References

872 Abrantes, F.: Diatom assemblages as upwelling indicators in surface sediments off
873 Portugal, *Mar. Geol.*, 85(1), 15–39, doi:10.1016/0025-3227(88)90082-5, 1988.

874

875 Ancapichún, S. and Garcés-Vargas, J.: Variability of the Southeast Pacific Subtropical
876 Anticyclone and its impact on sea surface temperature off north-central Chile
877 Variabilidad del Anticiclón Subtropical del Pacífico Sudeste y su impacto sobre
878 la temperatura superficial del mar frente a la costa centro-norte de Chile, *Cienc. Mar.*,
879 41(1), 1–20, doi:10.7773/cm.v41i1.2338, 2015.

880

881 Appleby, P. G. and Oldfield, F.: The calculation of lead-210 dates assuming a constant
882 rate of supply of unsupported ^{210}Pb to the sediment, *Catena*, 5(1), 1–8,
883 doi:10.1016/S0341-8162(78)80002-2, 1978.

884

885 Bevington, P. and Robinson, K. (Eds.): Error analysis. In: *Data Reduction and Error
886 Analysis for the Physical Sciences*, WCB/McGraw-Hill, USA, 38–52, 1992

887

888 Blanco, J.L., Carr, M-E., Thomas, A.C. and Strub, T.: Hydrographic conditions off
889 northern Chile during the 1996–1998 La Niña and El Niño events, *J. Geophys. Res.*,
890 107, C3, 3017, 10.1029/2001JC001002, 2002.

891

892 Blott, S. J. and Pye, K.: Gradistat: A Grain Size Distribution and Statistics Package for
893 the Analysis of Unconsolidated Sediments, *Earth Surf. Process. Landforms*, 26, 1237–
894 1248, doi:10.1002/esp.261, 2001.

895

896 Böning, P., Brumsack, H-J., Schnetger, B. and Grunwald, M.: Trace element

897 signatures of Chilean upwelling sediments at 36°S, *Mar. Geol.*, 259, 112–
898 121, 2009.
899
900 Böning, P., Shaw, T., Pahnke, K., Brumsack H-J.: Nickel as indicator of fresh organic
901 matter in upwelling sediments. *Geochim. Cosmochim. Ac.*, 162, 99–108, 2015.
902 Braconnot, P., Luan, Y., Brewer, S. and Zheng, W.: Impact of Earth's orbit and
903 freshwater fluxes on Holocene climate mean seasonal cycle and ENSO characteristics,
904 *Clim. Dyn.*, 38, 1081–1092, doi: 10.1007/s00382-011-1029-x, 2012.
905
906 Cardich, J., Sifeddine, A., Salvattecchi, R., Romero, D., Briceño-Zuluaga, F., Graco, M.,
907 Anculle, T., Almeida, C. and Gutiérrez, D.: Multidecadal Changes in Marine
908 Subsurface Oxygenation Off Central Peru During the Last ca. 170 Years, *Front. Mar.*
909 *Sci.*, 6(270), 1–16, doi: 10.3389/fmars.2019.00270, 2019.
910
911 Calvert, S. E. and Pedersen, T. F.: Chapter Fourteen Elemental Proxies for
912 Palaeoclimatic and Palaeoceanographic Variability in Marine Sediments: Interpretation
913 and Application, *Dev. Mar. Geol.*, 1(7), 567–644, doi:10.1016/S1572-5480(07)01019-6,
914 2007.
915
916 Carré, M., Sachs, J.P., Purca, S., Schauer, A.J. and Braconnot, P., Falcón, R.A., Julien,
917 M., Lavallée, D.: Holocene history of ENSO variance and asymmetry in the eastern
918 tropical Pacific, *Science* 345, 1045–1048. DOI: 10.1126/science.1255768. 2014.
919
920 Carré, M., Jackson, D., Maldonado, A., Chase, B.M. and Sachs, J.P.: Variability of 14C
921 reservoir age and air–sea flux of CO₂ in the Peru–Chile upwelling region during the
922 past 12,000 years, *Quat. Res.*, 85, 87–93, 2016.
923
924 Chaillou, G., Anschutz, P., Lavaux, G., Schäfer, J. and Blanc, G.: The distribution of
925 Mo, U, and Cd in relation to major redox species in muddy sediments of the Bay of
926 Biscay, *Mar. Chem.*, 80(1), 41–59, doi:10.1016/S0304-4203(02)00097-X, 2002.
927
928 Colodner, D., Sachs, J., Ravizza, G., Turekian, K. K. and Boyle, E.: The geochemical
929 cycle of Re: a reconnaissance, *Earth Planet. Sci. Lett.*, 117, 205–221, doi:10.1016/0012-
930 821X(93)90127-U, 1993.

Comentario [A22]: New reference

931
932 Croquette, M., Eldin, G., Grados, C. and Tamayo, M.: On differences in satellite winds
933 product and their effects in estimating coastal upwelling processes in the South-east
934 Pacific, *Geophys. Res. Lett.*, 34 L11 608, doi: 10.1029/2006GL027538. 2007.
935
936 Crusius, J., Calvert, S., Pedersen, T. and Sage, D.: Rhenium and molybdenum
937 enrichments in sediments as indicators of oxic, suboxic and sulfidic conditions of
938 deposition, *Earth Planet. Sci. Lett.*, 145(1–4), 65–78, doi:10.1016/S0012-
939 821X(96)00204-X, 1996.
940
941 Daneri, G., Dellarossa, V., Quiñones, R., Jacob, B., Montero, P. and Ulloa, O.: Primary
942 production and community respiration in the Humboldt Current System off Chile and
943 associated oceanic areas, *Mar. Ecol. Prog. Ser.*, 197, 41–49, doi:10.3354/meps197041,
944 2000.
945
946 De Pol-Holz, R., Ulloa, O., Dezileau, L., Kiser, J., Lamy, F., Hebbeln, D.: Melting of
947 the Patagonian Ice Sheet and deglacial perturbations of the nitrogen cycle in the eastern
948 South Pacific, *Geophys. Res. Lett.*, 33, L04704, doi: 10.1029/2005GL024477, 2006.
949
950 De Pol-Holz, R., Ulloa, O., Lamy, F., Dezileau, L., Sabatier, P., and Hebbeln, D.: Late
951 Quaternary variability of sedimentary nitrogen isotopes in the eastern South Pacific
952 Ocean, *Paleoceanography*, 22, PA2207, doi: 10.1029/2006 PA001308, 2007.
953
954 De Pol-Holz, R., Robinson, R.S., Hebbeln, D., Sigman, D.M., Ulloa, O.; Controls on
955 sedimentary nitrogen isotopes along the Chile margin, *Deep Sea Res. Part II: Topical
956 Studies in Oceanography*, 56, 1042–1054, <https://doi.org/10.1016/j.dsr2.2008.09.014>,
957 2009.
958
959 Dezileau, L., Ulloa, O., Hebbeln, D., Lamy, F., Reys, J. L. and Fontugne, M.: Iron
960 control of past productivity in the coastal upwelling system off the Atacama Desert,
961 Chile, *Paleoceanography*, 19(3), doi:10.1029/2004PA001006, 2004.
962
963 Dymond, J., Suess, E. and Lyle, M.: Barium in deep-sea sediment: A geochemical
964 proxy for paleoproductivity, *Paleoceanography*, 7(2), 163–181, 1992.

965
966 Escribano, R., Daneri, G., Farías, L., Gallardo, V. A., González, H. E., Gutiérrez, D.,
967 Lange, C. B., Morales, C. E., Pizarro, O., Ulloa, O. and Braun, M.: Biological and
968 chemical consequences of the 1997-1998 El Niño in the Chilean coastal upwelling
969 system: A synthesis, *Deep. Res. Part II Top. Stud. Oceanogr.*, 51(20–21), 2389–2411,
970 doi:10.1016/j.dsr2.2004.08.011, 2004.
971
972 Espinoza-Morriberón, D., Echevin, V., Colas, F., Tam, J., Gutierrez, D., Graco, M.,
973 Ledesma, J. and Quispe-Ccalluari, C.: Oxygen variability during ENSO in the Tropical
974 South Eastern Pacific, *Front. Mar. Sci.*, 5(526), 1–20, doi: 10.3389/fmars.2018.00526,
975 2019.
976
977 Faegri, K. and Iversen, J.: *Textbook of pollen analysis, IV*. The Blackburn Press, New
978 Jersey, 328 pp., 1989.
979
980 Figueroa, D. and Moffat, D.: On the influence of topography in the induction of coastal
981 upwelling along the Chilean coast, *Geophys. Res. Lett.* 27, 3905-3908, 2000.
982
983 Flynn, W. W.: The determination of low levels of polonium-210 in environmental
984 materials, *Anal. Chim. Acta*, 43, 221–227, 1968.
985
986 Frenger, I., Bianchi, D., Sührenberg, C., Oeschies, A., Dunne, J., Deutsch, C., Galbrath,
987 E. and Schütte, F.: Biogeochemical role of subsurface coherent eddies in the ocean:
988 Tracer cannonballs, hypoxic storms, and microbial stewpots?, *Global Biogeochem. Cy.*,
989 32, 226–249. <https://doi.org/10.1002/2017GB005743>, 2018.
990
991 Gallardo, M.A., González, A., Ramos, M., Mujica, A., Muñoz, P., Sellanes, J. and
992 Yannicelli, B.: Reproductive patterns in demersal crustaceans from the upper boundary
993 of the OMZ off north-central Chile, *Cont. Shelf. Res.* 141, 26–37, 2017.
994
995 Ganeshram, R.S., Pedersen, T. F., Calvert, S.G., McNeill, G. and Fontugne, M.:
996 Glacial-interglacial variability in denitrification in the world's oceans: Causes and
997 consequences, *Paleoceanography*, 15(4), 361– 376, 2000.
998

Comentario [A23]: New reference

Comentario [A24]: New reference

999 Garreaud, R., Barichivich, J., Christie, D. and Maldonado, A.: Interannual variability of
1000 the coastal fog at Fray Jorge relict forest in semiarid Chile, *Journal of Geophysical*
1001 *Research*. Vol 113. G04011, doi:10.1029/2008JG000709. 2008.
1002
1003 Garreaud, R., Vuille. M., Compagnucci, R. and Marengo, J.: Present-day South
1004 American climate, *Palaeogeogr. Palaeocl.*, 281, 180-195,
1005 doi:10.1016/j.palaeo.2007.10.032, 2009
1006
1007 Gergis, J.L. and Fowler, A.M.: A history of ENSO events since A.D. 1525: implications
1008 for future climate change, *Clim. Change*, 92,343–387, doi: 10.1007/s10584-008-9476-z,
1009 2009.
1010
1011 Govin, A., Holzwarth, U., Heslop, D., Ford Keeling, L., Zabel, M., Mulitza, S., Collins,
1012 J. A. and Chiessi, C. M.: Distribution of major elements in Atlantic surface sediments
1013 (36°N-49°S): Imprint of terrigenous input and continental weathering, *Geochemistry,*
1014 *Geophys. Geosystems*, 13(1), 1–23, doi:10.1029/2011GC003785, 2012.
1015
1016 Grimm, E.: CONISS: a fortran 77 program for stratigraphically constrained cluster
1017 analysis by the method of incremental sum of squares, *Comput. and Geosci.* 13–35,
1018 1987.
1019
1020 Gutiérrez, D., Sifedine, A., Reyss, J.L., Vargas, G., Velazco, F., Salvattecí, R., Ferreira,
1021 V., Ortlieb, L., Field, D., Baumgartner, T., Boussafir, M., Boucher, H., Valdés, J.,
1022 Marinovic, L., Soler, P. and Tapia, P: Anoxic sediments off Central Peru record
1023 interannual to multidecadal changes of climate and upwelling ecosystem during the last
1024 two centuries, *Adv. Geosci.* 6, 119–125, 2006.
1025
1026 Gutiérrez, D., Enríquez, E., Purca, S., Quipuzcoa, L., Marquina, R., Flores, G. and
1027 Graco, M.: Oxygenation episodes on the continental shelf of central Peru: Remote
1028 forcing and benthic ecosystem response, *Prog. Oceanogr.*, 79, 177–189, 2008.
1029
1030 Gutiérrez, D., Sifedine, A., Field, D.B., Ortlieb, L., Vargas, G., Chávez, F.P., Velazco,
1031 F., Ferreira, V., Tapia, P., Salvattecí, R., Boucher, H., Morales, M.C., Valdés, J., Reyss,
1032 J-L., Campusano, A., Boussafir, M., Mandeng-Yogo, M., García, M., and Baumgartner,

1033 T.: Rapid reorganization in ocean biogeochemistry off Peru towards the end of the Little
1034 Ice Age, *Biogeosciences*, 6, 835–848, 2009.

1035

1036 Hansen, H. P. and Koroleff, F.: Determination of nutrients. In *Methods of Seawater*
1037 *Analysis*. Grasshoff, K., Kremling, K. and Ehrhardt, M. (Eds.), Wiley-VCH Verlag
1038 GmbH, Weinheim, Germany, 159–228, 1999.

1039

1040 Haug, G.H., Hughen, K.A., Sigman, D.M., Peterson, L.C. and Röhl, U.: Southward
1041 Migration of the Intertropical Convergence Zone through the Holocene, *Sci.* 293, 1304–
1042 1307, 2001.

1043

1044 Hebbeln, D., Marchant, M., Freudenthal, T. and Wefer, G.: Surface distribution along
1045 the Chilean continental slope related to upwelling and productivity, *Mar.*
1046 *Geol.*, 164, 119–137, 2000.

1047

1048 Hebbeln, D., Marchant, M. and Wefer, G.: Paleoproductivity in the southern Peru ^
1049 Chile Current through the last 33 000 yr, *Mar. Geol.*, 186, 2002.

1050

1051 Helly, J. and Levin. L.: Global distribution of naturally occurring marine hypoxia on
1052 continental margin, *Deep-Sea Res. Pt. I*, 51, 1159-1168, 2004.

1053

1054 Heusser, C. J. and Moar, N. T.: Pollen and spores of chile: Modern types of the
1055 pteridophyta, gymnospermae, and angiospermae, *New Zeal. J. Bot.*, 11(2), 389–391,
1056 doi:10.1080/0028825X.1973.10430287, 1973.

1057

1058 Jenny, B., Valero-Garcés, B.L., Urrutia, R., Kelts, K., Veit, H., Appleby, P.G., Geyh,
1059 M.: Moisture changes and fluctuations of the Westerlies in Mediterranean
1060 Central Chile during the last 2000 years: The Laguna Aculeo record (33°50'S, *Quat.*
1061 *Int.* 87, 3–18, 2002.

1062

1063 Jenny, B., Wilhelm, D. and Valero-Garcés, B.L.: The Southern Westerlies in Central
1064 Chile: Holocene precipitation estimates based on a water balance model for Laguna
1065 Aculeo (33°50'S), *Clim. Dynam.*, 20, 269–280, DOI 10.1007/s00382-002-0267-3,
1066 2003.

1067
1068 Kaiser, J., Schefuß, E., Lamy, F., Mohtadi, M. and Hebbeln, D.: Glacial to Holocene
1069 changes in sea surface temperature and coastal vegetation in north central Chile: high
1070 versus low latitude forcing, *Quat. Sci. Rev.*, 27, 2064–2075, 2008.
1071
1072 Koutavas, A. and Joannides, S.: El Niño–Southern Oscillation extrema in the Holocene
1073 and Last Glacial Maximum, *Paleoceanography*, 27, PA4208,
1074 doi:10.1029/2012PA002378, 2012.
1075
1076 Koutavas, A., de Menocal, P.B., Olive, G.C. and Lynch-Stieglitz, J.: Mid-Holocene El
1077 Niño–Southern Oscillation (ENSO) attenuation revealed by individual foraminifera in
1078 eastern tropical Pacific sediments, 34(12), 993–996, doi: 10.1130/G22810A, 2006.
1079
1080 Koutavas, A., and Lynch-Stieglitz, J.: Variability of the marine ITCZ over the
1081 Eastern Pacific during the past 30,000 years. Regional Perspective and Global Context,
1082 in: *The Hadley Circulation*, Diaz, H.F., and Bradley, R.S., Eds. Chapter 12, *Advances in*
1083 *Global Change Research book series (Aglo, volume 21)*, 347–369, 2004.
1084
1085 Lamy F., Hebbeln, D. and Wefer, G.: High-Resolution Marine Record of Climatic
1086 Change in Mid-latitude Chile during the Last 28,000 Years Based on Terrigenous
1087 Sediment Parameters, *Quat. Res.*, 51, 83–93, 1999.
1088
1089 Lamy F., Hebbeln, D., Röhl, U. and Wefer, G.: Holocene rainfall variability in southern
1090 Chile: a marine record of latitudinal shifts of the Southern Westerlies, *Earth Planet Sc.*
1091 *Lett.*, 185, 369–382, 2001.
1092
1093 Lamy, F., Kilian, R., Arz, H.W., Francois J-P., Kaiser, J., Prange, M. and Steinke, T.:
1094 Holocene changes in the position and intensity of the southern westerly wind belt, *Nat.*
1095 *Geosci.*, 3, 695–699, 2010.
1096
1097 Little, S. H., Vance, D., Walker-Brown, C. and Landing, W. M.: The oceanic mass
1098 balance of copper and zinc isotopes, investigated by analysis of their inputs, and outputs
1099 to ferromanganese oxide sediments, *Geochim. Cosmochim. Ac.*, 125, 673–693,
1100 doi:10.1016/j.gca.2013.07.046, 2014.

Comentario [A25]: New reference

1101
1102 Maldonado, A. and Rozas, E.: Clima y Paleoambientes durante el Cuaternario Tardío en
1103 la Región de Atacama, in Libro Rojo de la Flora Nativa y de los Sitios Prioritarios para
1104 su Conservación: Región de Atacama, pp. 293–304., 2008.
1105
1106 Maldonado, A. and Villagrán, C.: Paleoenvironmental changes in the semiarid coast of
1107 Chile (~32°S) during the last 6200 cal years inferred from a swamp-forest pollen
1108 record, *Quat. Res.*, 58, 130–138, 2002.
1109
1110 Maldonado, A. and Villagrán, C.: Climate variability over the last 9900 cal yr BP from
1111 a swamp forest pollen record along the semiarid coast of Chile, *Quat. Res.*, 66(2), 246–
1112 258, doi:10.1016/j.yqres.2006.04.003, 2006.
1113
1114 Mazzullo, J., Leschak, P. and Prusak, D.: Sources and distribution of late Quaternary
1115 silt in the surficial sediment of the northeastern continental shelf of the United States,
1116 *Mar. Geol.*, 78:241–254, 1988.
1117
1118 McManus, J., Berelson, W. M., Severmann, S., Poulson, R. L., Hammond, D. E.,
1119 Klinkhammer, G. P., and Holm, C.: Molybdenum and uranium geochemistry in
1120 continental margin sediments: Paleoproxy potential, *Geochim. Cosmochim. Ac.*, 70,
1121 4643–4662, 2006.
1122
1123 Merino-Campos, V., De Pol-Holz, R., Southon, J., Latorre, C., Collado-Fabbri, S.:
1124 Marine radiocarbon reservoir age along the Chilean continental margin, *Radiocarbon*,
1125 81, 1–16, doi:10.1017/RDC.2018.81, 2018.
1126
1127 Mollier-Vogel, E., Martinez, P., Blanz, T., Robinson, R., Desprat, S., Etourneau, J.,
1128 Charlier, K., Schneider, R. R.: Mid-Holocene deepening of the Southeast Pacific
1129 oxycline, *Global Planet Change*, 172, 365–373, 2019.
1130
1131 Montecinos, A., and Aceituno, P.: Seasonality of the ENSO-Related Rainfall Variability
1132 in Central Chile and Associated Circulation Anomalies, *J. Climate.*, 16, 281–296, 2003.
1133

1134 Montecinos, S., Gutiérrez, J. R., López-Cortés, F. and López, D.: Climatic
1135 characteristics of the semi-arid Coquimbo Region in Chile, *J. Arid Environ.*, 126, 7–11,
1136 doi:10.1016/j.jaridenv.2015.09.018, 2016.

1137

1138 Moraga-Opazo, J., Valle-Levinson, A., Ramos, M. and Pizarro-Koch, M.: Upwelling-
1139 Triggered near-geostrophic recirculation in an equatorward facing embayment, *Cont.*
1140 *Shelf Res.*, 31, 1991–1999, 2011.

1141

1142 Morford, J. and Emerson, S.: The geochemistry of redox sensitive trace metals in
1143 sediments, *Geochim. Cosmochim. Ac.*, 63, 11/12, 1735–1750, 1999.

1144

1145 Mortlock, R. A. and Froelich, P. N.: A simple method for the rapid determination of
1146 biogenic opal in pelagic marine sediments, *Deep Sea Res. Part A, Oceanogr. Res. Pap.*,
1147 36(9), 1415–1426, doi:10.1016/0198-0149(89)90092-7, 1989.

1148

1149 Muñoz, P., Dezileau, L., Lange, C., Cárdenas, L., Sellanes, J., Salamanca, M.,
1150 Maldonado A.: Evaluation of sediment trace metal records as paleoproductivity and
1151 paleoxygenation proxies in the upwelling center off Concepción, Chile (36° S). *Prog.*
1152 *Oceanogr.*, Special Issue 92-95, 66-80, 2012.

1153

1154 Nameroff, T., Balistrieri, L. and Murray, W.: Suboxic trace metals geochemistry in the
1155 eastern tropical North Pacific, *Geochim Cosmochim Ac.*, 66(7), 1139–1158, 2002.

1156

1157 Ohnemus, D. C. and Lam, P. J.: Cycling of lithogenic marine particles in the US
1158 GEOTRACES North Atlantic transect, *Deep. Res. Part II Top. Stud. Oceanogr.*, 116,
1159 283–302, doi:10.1016/j.dsr2.2014.11.019, 2015.

1160

1161 Ortega, C., Vargas, G., Rutllant, J.A., Jackson, D. and Méndez, C.: Major hydrological
1162 regime change along the semiarid western coast of South America during the early
1163 Holocene, *Quaternary Res.*, 78, 513-527, 2012.

1164

1165 Ortega, C., Vargas, G., Rojas, M., Rutllant, J.A., Muñoz, P., Lange, C.B., Pantoja, S.,
1166 Dezileau, L. and Ortlieb, L.: Extreme ENSO-driven torrential rainfalls at the southern
1167 edge of the Atacama Desert during the late Holocene and their projection into the 21th

1168 century, GloPlaCha, 175, 226 – 237, [https://doi.org/ 10.1016/j.gloplacha.2019.02.011](https://doi.org/10.1016/j.gloplacha.2019.02.011),
1169 2019.
1170
1171 Paytan, A.: Ocean paleoproductivity, Encyclopedia of Paleoclimatology and Ancient
1172 Environments, Encyclopedia of Earth Science Series, Gornitz, V. (Ed.), Kluwer
1173 Academic Publishers. 2008.
1174
1175 Peacock, C.L. and Sherman, D.M.: Copper(II) sorption onto goethite, hematite and
1176 lepidocrocite: a surface complexation model based on ab initio molecular geometries
1177 and EXAFS spectroscopy, *Geochim. Cosmochim. Ac.*, 68, 2623–2637, 2004.
1178
1179 Pizarro, O., Hormazabal, S., Gonzalez, A. and Yañez, E.: Variabilidad
1180 del viento, nivel del mar y temperatura en la costa norte de Chile, *Invest.*
1181 *Mar.*, 22, 85–101, 1994.
1182
1183 Pizarro, O., Shaffer, G., Dewitte, B. and Ramos, M.: Dynamics of seasonal and
1184 interannual variability of the Peru-Chile Undercurrent, *Geophys. Res. Lett.*, 29(12), 28–
1185 31, doi:10.1029/2002GL014790, 2002.
1186
1187 Pizarro-Koch, M., Pizarro, O., Dewitte, B., Montes, I., Ramos, M., Paulmier, A. and
1188 Garçon, V.: Seasonal variability of the southern tip of the Oxygen Minimum Zone in
1189 the eastern South Pacific (30°–38°S): A modeling study, *J. Geophys. Res. Oceans*, 124,
1190 <https://doi.org/10.1029/2019JC015201>, 2019.
1191
1192 Quintana, J.M. and Aceituno, P.: Changes in the rainfall regime along the extratropical
1193 west coast of South America (Chile): 30–43° S, *Atmosfera*, 25(1), 1 – 22, 2012.
1194
1195 Ramos, M., Pizarro, O., Bravo, L. and Dewitte, B.: Seasonal variability of the permanent
1196 thermocline off northern Chile, *Geophys. Res. Lett.*, 33, L09608,
1197 doi:10.1029/2006GL025882, 2006.
1198
1199 Ramos, M., Dewitte, B., Pizarro, O. and Garric, G.: Vertical propagation of
1200 extratropical Rossby waves during the 1997–1998 El Niño off the west coast of South
1201 America in a medium-resolution OGCM simulation, *J. Geophys. Res.*, 113, C08041,

Comentario [A26]: New reference

1202 doi:10.1029/2007JC004681, 2008.
1203
1204 Rahn, D.A. and Garreaud, R.A.: A synoptic climatology of the near-surface wind along
1205 the west coast of South America. *Int. J. Climatol.*, 34(3), 780–792, doi:
1206 10.1002/joc.3724, 2013.
1207
1208 Reimer, P. J., Bard, E., Bayliss, A., Beck, J. W., Blackwell, P. G., Ramsey, C. B., Buck,
1209 C. E., Cheng, H., Edwards, R. L., Friedrich, M., Grootes, P. M., Guilderson, T. P.,
1210 Hafliðason, H., Hajdas, I., Hatté, C., Heaton, T. J., Hoffmann, D. L., Hogg, A. G.,
1211 Hughen, K. A., Kaiser, K. F., Kromer, B., Manning, S. W., Niu, M., Reimer, R. W.,
1212 Richards, D. A., Scott, E. M., Southon, J. R., Staff, R. A., Turney, C. S. M. and van der
1213 Plicht, J.: IntCal13 and Marine13 Radiocarbon Age Calibration Curves 0–50,000 Years
1214 cal BP, *Radiocarbon*, 55(4), 1869–1887, doi:10.2458/azu_js_rc.55.16947, 2013.
1215
1216 Rein, B., Lückge, A., Reinhardt, L., Sirocko, F., Wolf, A. and Dullo, W-C.: El Niño
1217 variability off Peru during the last 20,000 years, *Paleoceanogr.*, PA4003,
1218 doi:10.1029/2004PA001099, 2005
1219
1220 Rutlland, J. and Fuenzalida, H.: Synoptic aspects of the central Chile Rainfall variability
1221 associated with the southern oscillation, *Int. J. Climatol.*, 11, 63 – 76, 1991.
1222
1223 Rutlland, J. and Montecino, V.: Multiscale upwelling forcing cycles and biological
1224 response off northcentral Chile, *Rev. Chil. Hist. Nat.*, 7, 217–231, 2002
1225
1226 Sabatier, P., Dezileau, L., Blanchemanche, P., Siani, G., Condomines, M., Bentaleb, I.
1227 and Piquès, G.: Holocene variations of radiocarbon reservoir ages in a mediterranean
1228 lagoonal system, *Radiocarbon*, 52(1), 91–102, doi:10.1017/S0033822200045057, 2010.
1229
1230 Sadler, P.M.: The Influence of Hiatuses on Sediment Accumulation Rates, *GeoResearch*
1231 *Forum*, 5, 15–40, 1999.
1232
1233 Saito, C., Noriki, S. and Tsunogai, S.: Particulate flux of Ai, a component of land
1234 origin, in the western North Pacific, *Deep-Sea Res.*, 39, 1315–1327, 1992.
1235

1236 Salvattecí, R., Gutiérrez, D., Field, D., Sifeddine, A., Ortlieb, L., Bouloubassi, I.,
1237 Boussafir, M., Boucher, H. and Cetin, F.: The response of the Peruvian Upwelling
1238 Ecosystem to centennial-scale global change during the last two millennia, *Clim. Past*,
1239 10(2), 715–731, doi:10.5194/cp-10-715-2014, 2014.

1240

1241 Salvattecí, R., Gutiérrez, D., Sifeddine, A., Ortlieb, L., Druffel, E., Boussafir, M.,
1242 Schneider, R.: Centennial to millennial-scale changes in oxygenation and productivity
1243 in the Eastern Tropical South Pacific during the last 25,000 years,
1244 *Quat. Sci. Rev.*, 131, 102–117, 2016.

1245

1246 Sandweiss, D.H., Maasch, K.A., Andrus, C. Fred T., Reitz, E.J., Richardson III, J.B.,
1247 Riedinger-Whitmore, M., and Rollins, H.B.: Mid-Holocene climate and culture change
1248 in coastal Peru, Chapter 2, In: *Climate Change and Cultural Dynamics: A Global
1249 Perspective on Mid-Holocene Transitions*, Anderson, D.G., Maasch, K.A., and
1250 Sandweiss, D.H. (Eds.), Elsevier Inc., 25–50, 2007.

1251

1252 Schrader H. J. and Gersonde, R.: Diatoms and silicoflagellates, *Utrecht Micropaleontol.*
1253 *Bull.* 17, 129–176, 1978.

1254

1255 Sellanes, J., Quiroga, E., Neira, C., Gutiérrez, D.: Changes of macrobenthos
1256 composition under different ENSO cycle conditions on the continental shelf off central
1257 Chile, *Cont. Shelf. Res.* 27, 1002 –1016, 2007.

1258

1259 Shaffer, G., Pizarro, O. Djurfeldt, L., Salinas, S. and Rutllant, J.: Circulation and low-
1260 frequency variability near the Chilean coast: Remotely forced fluctuations during the
1261 1991– 92 El Niño, *J. Phys. Oceanogr.*, 27, 217– 235, 1997.

1262

1263 Shaffer, G., Hormazabal, S., Pizarro, O. and S. Salinas.: Seasonal and interannual
1264 variability of currents and temperature over the slope of central Chile, *J. Geophys. Res.*,
1265 104, C12, 29,951-29,961, 1999.

1266

1267 Scholz, F., Hensen, C., Noffke, A., Rohde, A., Liebetrau, V., Wallmann, K.: Early
1268 diagenesis of redox-sensitive trace metals in the Peru upwelling area – response to

1269 ENSO-related oxygen fluctuations in the water column, *Geochim. Cosmochim. Ac.*, 75,
1270 7257–7276, 2011.
1271
1272 Siebert, C., Nägler, T.F., von Blackenburg, F. and Kramers, J.D.: Molybdenum
1273 isotope records as a potential new proxy for paleoceanography, *Earth Planet. Sci. Lett.*,
1274 6643, 1–13, 2003.
1275
1276 Sigman, D.M., Karsh, K.L. and Casciotti, K.L.: Ocean process tracers: nitrogen isotopes
1277 in the ocean. *Encyclopedia of ocean science*, 2nd edn Elsevier, Amsterdam, 2009.
1278
1279 Sundby, B., Martinez, P. and Gobeil, C.: Comparative geochemistry of cadmium,
1280 rhenium, uranium, and molybdenum in continental margin sediments, *Geochim.*
1281 *Cosmochim. Ac.*, 68, 2485–2493, 2004.
1282
1283 Sweeney, R. E. and Kaplan I. R.: Natural abundances of ¹⁵N as a source indicator of
1284 nearshore marine sedimentary and dissolved nitrogen, *Mar. Chem.*, 9, 81– 94, 1980.
1285
1286 Thiel, M., Macaya, E.C., Acuña, E., Artz, W.F., Bastias. H., Brokordt. K., Camus,
1287 P.A., Castilla, J.C., Castro, L.R., Cortés, M., Dumont, C.P., Escribano, R., Fernandez,
1288 M., Gajardo, J.A., Gaymer, C.F., Gómez, I, González, A.E., González, H.E., Haye, P.,
1289 Illanes, J.E., Iriarte, J.L., Lancellotti, D.A., Luna-Jorquera, G., Luxoro, C., Manriquez,
1290 P.H., Marín, V., Muñoz, P., Navarrete, S.A., Pérez, E., Poulin, E., Sellanes, J.,
1291 Sepúlveda, H.H., Stotz, W., Tala, F., Thomas, A., Vargas, C.A., Vásquez, J.A., Vega,
1292 J.M.: The Humboldt Current system of Northern and Central Chile: Oceanographic
1293 processes, ecological interactions and socioeconomic feedback, *Oceanogr. Mar. Biol.*
1294 *An Annual Review*, 45, 195–344, 2007.
1295
1296 Torres, M. E., Brumsack, H. J., Bohrman, G. and Emeis, K. C.: Barite front in
1297 continental margin sediments: a new look at barium remobilization in the zone of
1298 sulfate reduction and formation of heavy barites in diagenetic fronts, *Chem. Geol.*, 127,
1299 125–139, 1996.
1300

1301 Torres, R., and Ampuero, P.: Strong CO₂ outgassing from high nutrient low chlorophyll
1302 coastal waters off central Chile (30°S): The role of dissolved iron, *Estuar. Coast. Shelf*
1303 *S.*, 83, 126–132, doi:10.1016/j.ecss.2009.02.030, 2009.

1304

1305 Toth, L.T., Aronson, R.B., Vollmer, S.V., Hobbs, J.W., Urrego, D.H., Cheng, H.,
1306 Enochs, I.C., Combsch, D.J., van Woesik, R., Macintyre, J.G.: ENSO Drove 2500-
1307 Year Collapse of Eastern Pacific Coral Reefs, *Science* 337, 81– 84, doi:
1308 10.1126/science.1221168, 2012

1309

1310 Tribovillard, N., Algeo, T. J., Lyons, T. and Riboulleau, A.: Trace metals as paleoredox
1311 and paleoproductivity proxies: an update, *Chem. Geol.*, 232, 12–32, 2006.

1312

1313 Ulloa, O., Escribano, R., Hormazabal, S., Quiñones, R.A., Gonzalez, R., Ramos, M.,:
1314 Evolution and biological effects of the 1997-98 El Niño in the upwelling ecosystem off
1315 northern Chile, *Geophys. Res. Lett.*, 28, 1591– 1594, 2001.

1316

1317 Ulloa, O., Canfield, D.E., DeLong, E.F., Letelier, R.L. and Stewart, F.J.: Microbial
1318 oceanography of anoxic oxygen minimum zones, *PNAS*, 109, 15996–16003,
1319 doi/10.1073/pnas.1205009109, 2012.

1320

1321 Vance, D., Archer, C., Bermin, J., Perkins, J., Statham, P. J., Lohan, M. C., Ellwood, M.
1322 J. and Mills, R. A.: The copper isotope geochemistry of rivers and the oceans, *Earth*
1323 *Planet. Sc. Lett.*, 274, 204–213, 2008.

1324

1325 Valle-Levinson, A., Moraga, J., Olivares, J. and Blanco, J. L.: Tidal and residual
1326 circulation in a semi-arid bay: Coquimbo Bay, Chile, *Cont. Shelf Res.*, 20, 2009–2018,
1327 2000.

1328

1329 Valle-Levinson, A. and Moraga-Opazo, J.: Observations of bipolar residual circulation
1330 in two equatorward-facing semiarid bays, *Cont. Shelf Res.*, 26(2), 179–193,
1331 doi:10.1016/j.csr.2005.10.002, 2006.

1332

1333 Van der Weijden, C.: Pitfalls of normalization of marine geochemical data using a
1334 common divisor, *Mar. Geol.*, 184, 167–187, 2002.

1335
1336 Vargas, G., Ortlieb, L., Pichon, J. J., Bertaux, J. and Pujos, M.: Sedimentary facies and
1337 high resolution primary production inferences from laminated diatomaceous sediments
1338 off northern Chile (23°S), *Mar. Geol.*, 211(1–2), 79–99,
1339 doi:10.1016/j.margeo.2004.05.032, 2004.
1340
1341 Vargas, G., Rutllant, J., Ortlieb, L.: ENSO tropical–extratropical climate
1342 teleconnections and mechanisms for Holocene debris flows along the hyperarid coast of
1343 western South America (17°–24°S), *Earth Planet. Sci. Lett.*, 249, 467–483, 2006.
1344
1345 Vargas, G., Pantoja, S., Rutllant, J., Lange, C. and Ortlieb, L.: Enhancement of coastal
1346 upwelling and interdecadal ENSO-like variability in the Peru-Chile Current since late
1347 19th century, *Geophys. Res. Lett.*, 34, L13607, 2007.
1348
1349 Vergara, O., Dewitte, B., Montes, I., Garçon, V., Ramos, M., Paulmier, A. and
1350 Pizarro, O.: Seasonal variability of the oxygen minimum zone off Peru in a high-
1351 resolution regional coupled model, *Biogeosciences*, 13, 4389–4410, doi:10.5194/bg-13-
1352 4389-2016, 2016.
1353
1354 Veit, H.: Southern Westerlies during the Holocene deduced from geomorphological and
1355 pedological studies in the Norte Chico, Northern Chile (27–33°S), *Palaeogeogr.,*
1356 *Palaeoclimatol., Palaeoecol.*, 123, 107–119, 1996.
1357
1358 Xu, G., Liu, J., Pei, S., Kong, X., Hu, G. and Gao, M.: Source identification of
1359 aluminum in surface sediments of the Yellow Sea off the Shandong Peninsula, *Acta*
1360 *Oceanol. Sin.*, 34(12), 147–153, doi:10.1007/s13131-015-0766-9, 2015.
1361
1362 Yang, S., and Oh, J-H.: Effects of modes of climate variability on wave power during
1363 boreal summer in the western North Pacific, *Sci. Rep.*, 10:5187, doi:10.1038/s41598-
1364 020-62138-0, 2020.
1365
1366 Zheng, Y., Anderson, R. F., van Geen, A. and Fleisheir, M.Q.: Preservation of non-
1367 lithogenic particulate uranium in marine sediments, *Geochim. Cosmochim. Ac.*, 66,
1368 3085–3092, 2002.

Comentario [A27]: New reference

1369

1370 **Acknowledgments**

1371 We would like to thank the R/V Stella Maris II crew of Universidad Católica del Norte
1372 for their help and support during field work. We extend our acknowledgements to the
1373 laboratory assistants of the Paleoceanography Lab at Universidad de Concepción for aid
1374 in the sample analyses, and to the assistants of the Oceanography Lab of Universidad
1375 Católica del Norte for aid in data analysis. We also wish to thank Dr. Olivier Bruguier
1376 of CNRS and his lab personnel for their assistance during ICPM analyses. We also
1377 express our gratitude to INNOVA 07CN13 IXM-150, FONDECYT 1180413 and
1378 FONDECYT 1170408. This manuscript was mainly funded by FONDECYT Project
1379 No. 1140851. Partial support from the COPAS Sur-Austral (CONICYT PIA PFB31)
1380 and FONDAP-IDEAL centers (No. 15150003) is also acknowledged.

1381

1382 **Author contributions:** PM prepared the manuscript with contributions from all co-
1383 authors. PM, LR and LD developed the proposal and conducted field work. AM, KA
1384 and MR assisted in field work in different campaigns. All authors participated in
1385 different laboratory work and data analysis, PM, LD and KA conducted metal and
1386 radioisotope analyses. MR analyzed physical data and graphs editing. MS helped with
1387 alpha counting on prepared samples. CM ran stable isotope and TOC analysis. LR, CL,
1388 PC, GS and KL assisted in specimen identifications of foraminifers and diatoms. AM
1389 and IJ identified pollen and assisted with the age modeling. GV analyzed physical
1390 properties of the sediments and contributed to writing and editing the manuscript.

1391

1392 **Competing interests.** The authors declare that they have no conflict of interest.

1393

1394

1395

1396

1397

1398

1399

1400

1401

1402

1403

1404

1405 **Tables**

1406

1407 Table 1. Radiocarbon dates for BGGC5 and BTGC8 sediment cores collected from
 1408 mixed planktonic foraminifera and monospecific benthic foraminifera (*Bolivina*
 1409 *plicata*), respectively. The ¹⁴C-AMS was performed at NOSAM-WHOI. The lab code
 1410 and conventional ages collected from each core section are indicated. For error
 1411 calculations see <http://www.whoi.edu/nosams/radiocarbon-data-calculations>.

Core identification	Material	Mass (mg)	Lab Code NOSAM	Modern fraction pMC	1σ error	Conventional Age BP	1σ error
Planktonic foraminifera							
BGGC5							
10-11	Mix	1.8	OS-122160	0.8895	0.0027	940	25
18-19	Mix	1.1	OS-122141	0.7217	0.0024	2,620	25
31-32	Mix	2.7	OS-122161	0.6590	0.0021	3,350	25
45-46	Mix	2.0	OS-122162	0.6102	0.0017	3,970	25
55-56	mix	1.6	OS-122138	0.5864	0.0025	4,290	35
66-67	mix	2.8	OS-122304	0.5597	0.0018	4,660	25
76-77	mix	2.6	OS-122163	0.4520	0.0016	6,380	30
96-97	mix	1.1	OS-122139	0.4333	0.0033	6,720	60
115-116	mix	4.7	OS-122164	0.3843	0.0016	7,680	35
Benthic foraminifera							
BTGC8							
5-6	<i>Bolivina plicata</i>	4.2	OS-130657	0.8953	0.0017	890	15
20-21	<i>Bolivina plicata</i>	7.7	OS-123670	0.7337	0.0021	2,490	25
30-31	<i>Bolivina plicata</i>	13.0	OS-123671	0.6771	0.0016	3,130	20
40-41	<i>Bolivina plicata</i>	11.0	OS-123672	0.6507	0.0019	3,450	25
50-51	<i>Bolivina plicata</i>	8.7	OS-123673	0.5877	0.0014	4,270	20
60-61	<i>Bolivina plicata</i>	13.0	OS-123674	0.5560	0.0018	4,720	25
71-72	<i>Bolivina plicata</i>	10.0	OS-123675	0.4930	0.0013	5,680	20
80-81	<i>Bolivina plicata</i>	7.3	OS-123676	0.4542	0.0012	6,340	20
90-91	<i>Bolivina plicata</i>	6.8	OS-123677	0.4259	0.0015	6,860	30
96-97	<i>Bolivina plicata</i>	6.8	OS-123678	0.3903	0.0013	7,560	25

1412

1413

1414

1415

1416

1417

1418

1419

1420 Table 2. Reservoir age estimation considering the ^{210}Pb age determined with the CRS
 1421 model (McCaffrey and Thomson, 1980) at selected depth sections of the core, as
 1422 compared with ^{14}C ages (y BP) from the marine 13.14 curve (Reimer et al., 2013),
 1423 according to Sabatier et al. (2010).

Core	Depth (cm)	Age from CRS model (AD) ^a	Age years BP ^b	^{14}C age Marine 13.14	^{14}C age BP from foram.	DR
BGGC5	10.5	1828	122	499±24	940±25	441±35
BTCG8	5.5	1908	42	448±23	890±15	442±27

^aAnno Domini

^bBefore present=1950

1424

1425

1426 Table 3. Concentration of elements in the Pachingo wetland sediments, considered as
 1427 lithogenic background for the study area. The values correspond to mean concentrations
 1428 in the surface sediments (0–3 cm).

Element	Metal/Al x 10 ³	s
Ca	686.5	139.3
Fe	591.3	84.5
P	8.6	0.7
Sr	5.7	0.6
Ba	5.6	0.1
Cu	0.258	0.019
Ni	0.174	0.005
U	0.020	0.003
Mo	0.020	0.003
Cd	0.0021	0.0003
Re	0.00004	0.00001

1429

1430

1431

1432

1433

1434

1435

1436

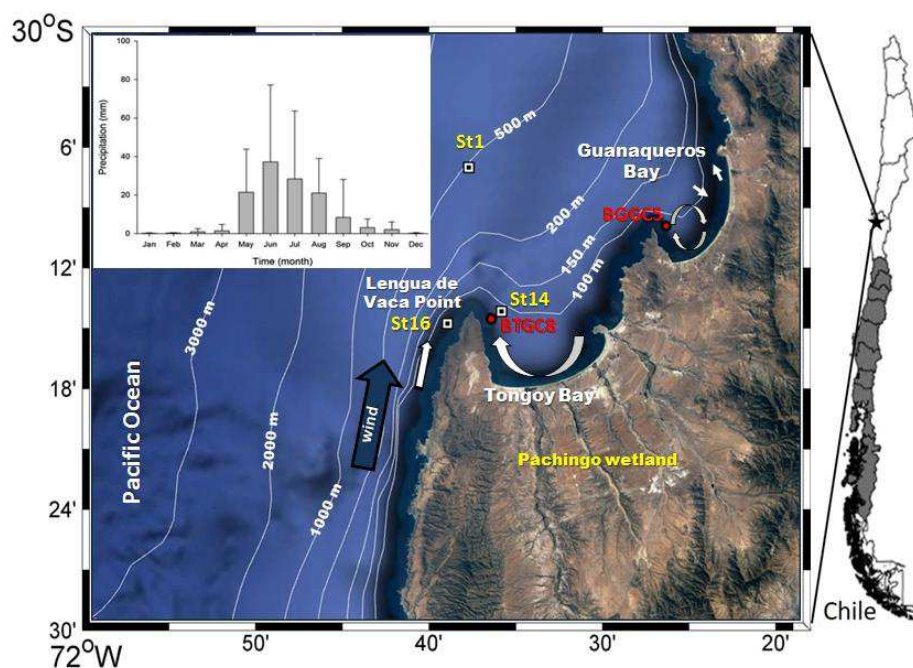
1437 Table 4. Spearman rank order correlations for geochemical data. Significant values

1438 > 0.8 are indicated in bold.

BGGC5																
	Al	P	K	Ca	Mn	Fe	Ni	Cu	Mo	Cd	Re	Sr	U	Ba	Opal	TOC
Al	1.00	-0.62	0.49	-0.48	0.64	0.60	-0.75	0.56	-0.10	-0.73	-0.08	-0.33	0.08	0.49	-0.52	-0.44
P		1.00	-0.31	0.37	-0.45	-0.56	0.56	-0.57	0.01	0.61	-0.11	0.39	-0.12	-0.20	0.49	0.24
K			1.00	-0.24	0.90	0.83	-0.29	0.47	0.28	-0.42	0.33	-0.12	0.50	0.26	-0.25	-0.19
Ca				1.00	-0.47	-0.50	0.44	-0.64	0.23	0.59	0.39	0.92	0.30	-0.60	0.18	0.32
Mn					1.00	0.94	-0.51	0.68	-0.01	-0.68	0.07	-0.32	0.24	0.43	-0.39	-0.31
Fe						1.00	-0.49	0.81	0.03	-0.70	0.11	-0.40	0.23	0.36	-0.37	-0.21
Ni							1.00	-0.51	0.49	0.91	0.35	0.25	0.26	-0.70	0.72	0.64
Cu								1.00	-0.12	-0.71	-0.06	-0.61	0.00	0.31	-0.39	-0.07
Mo									1.00	0.50	0.88	0.10	0.91	-0.48	0.33	0.36
Cd										1.00	0.36	0.42	0.27	-0.67	0.70	0.54
Re											1.00	0.27	0.92	-0.50	0.16	0.38
Sr												1.00	0.24	-0.36	0.05	0.17
U													1.00	-0.39	0.10	0.29
Ba														1.00	-0.30	-0.59
Opal															1.00	0.35
TOC																1.00
BTGC8																
	Al	P	K	Ca	Mn	Fe	Ni	Cu	Mo	Cd	Re	Sr	U	Ba	Opal	TOC
Al	1.00	-0.19	-0.17	-0.37	-0.02	-0.03	-0.39	-0.04	-0.39	0.02	-0.13	-0.58	-0.19	0.07	-0.41	-0.29
P		1.00	0.23	0.00	0.43	0.28	0.58	0.23	0.37	0.13	-0.04	0.30	0.14	-0.14	0.56	0.13
K			1.00	-0.02	0.54	0.41	0.43	0.22	-0.11	0.05	-0.04	0.19	-0.28	0.28	0.26	0.20
Ca				1.00	-0.33	-0.27	0.00	-0.23	0.39	0.01	0.33	0.50	0.47	-0.34	0.20	0.34
Mn					1.00	0.21	0.64	0.01	0.05	0.33	0.15	0.32	-0.02	0.24	0.32	0.00
Fe						1.00	0.13	0.71	-0.40	-0.48	-0.67	-0.37	-0.62	0.13	0.14	0.10
Ni							1.00	0.24	0.56	0.20	0.25	0.64	0.19	-0.16	0.80	0.45
Cu								1.00	-0.25	-0.68	-0.56	-0.22	-0.61	-0.10	0.21	0.37
Mo									1.00	0.45	0.59	0.66	0.69	-0.41	0.58	0.30
Cd										1.00	0.56	0.39	0.52	0.11	0.10	-0.12
Re											1.00	0.53	0.83	-0.16	0.13	0.17
Sr												1.00	0.58	-0.13	0.52	0.23
U													1.00	-0.19	0.21	0.00
Ba														1.00	-0.28	-0.42
Opal															1.00	0.39
TOC																1.00

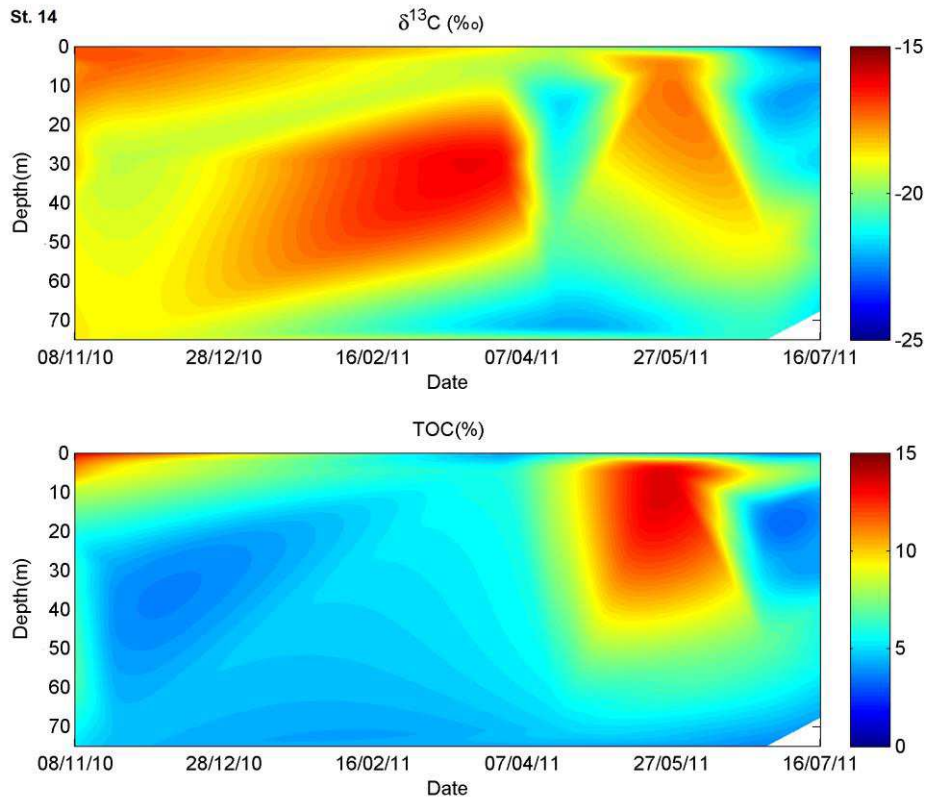
Figures

1439 Figure 1. Study area showing the positions of sampling stations. Sediment cores were
1440 retrieved from Guanaqueros Bay (BGGC5) and Tongoy Bay (BTGC8) at water depths
1441 of 89 and 85 m, respectively. Information of dissolved oxygen in the water column at
1442 St1 and St16 and that of suspended organic particles collected at St14 sampling sites
1443 was gathered in a previous project (INNOVA 07CN13 IXM-150). Monthly
1444 precipitation in mm (bars) (mean \pm SD; Montecinos et al., 2016). Schematic
1445 representation of the circulation in the bays (white arrows) and wind direction (blue
1446 arrow) is indicated, as obtained from Valle-Levinson and Moraga-Opazo (2006) and
1447 Moraga-Opazo et al. (2011).



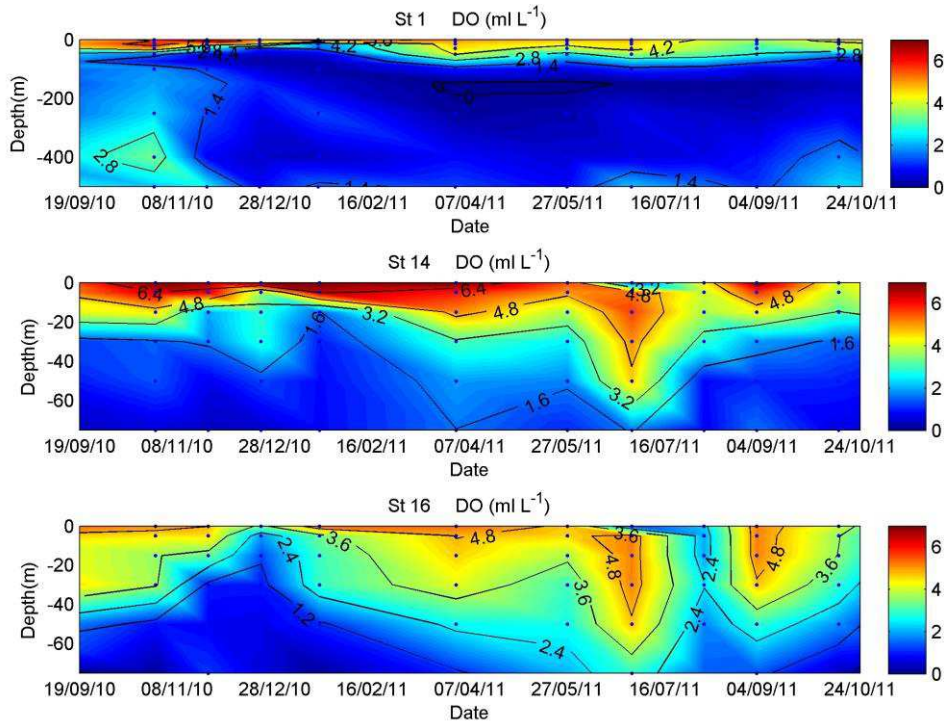
1448
1449
1450
1451
1452

1453 Figure 2. Suspended particulate matter composition (TOC% and $\delta^{13}\text{C}_{\text{org}}$) measured in
1454 the water column between October 2010 and October 2011, at station St14, Tongoy
1455 Bay, Coquimbo (30° S).



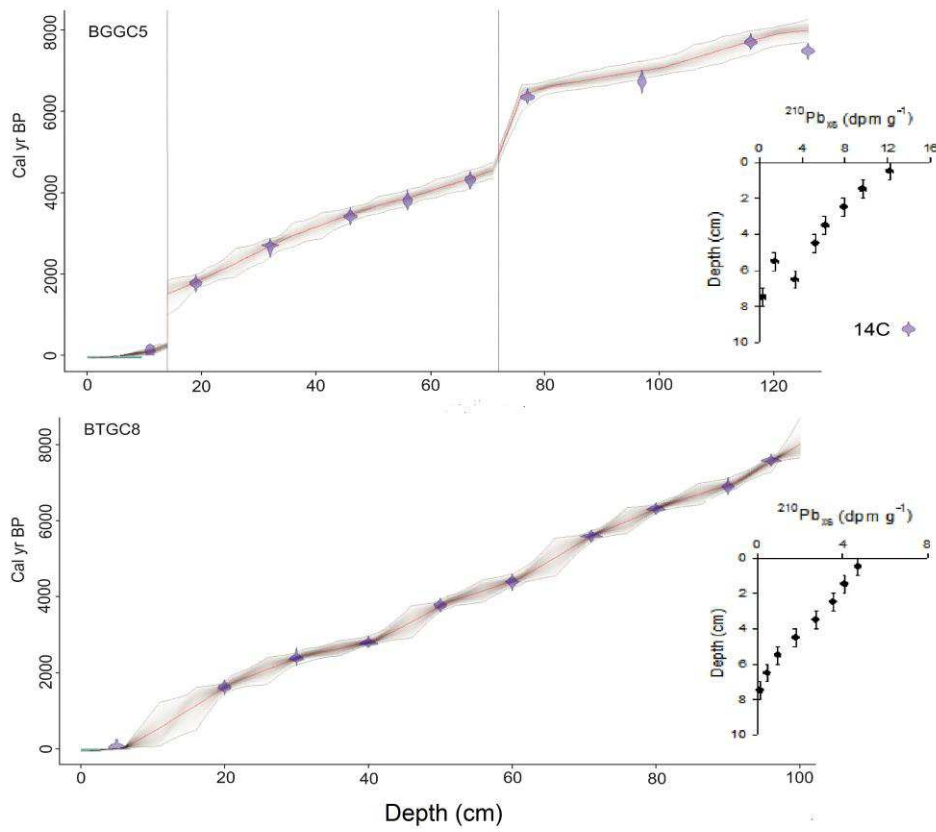
1456
1457
1458
1459
1460
1461
1462
1463
1464
1465
1466

1467 Figure 3. Dissolved oxygen time series in the water column measured between October
1468 2010 and January 2011, at stations St1, St14, and St16 off Tongoy Bay, Coquimbo
1469 (30° S).



1470
1471
1472
1473
1474
1475
1476
1477
1478
1479
1480
1481
1482
1483

1484 Figure 4. Age model based on ^{14}C -AMS and ^{210}Pb measurements. The timescale was
1485 obtained according to the Bacon age–depth modeling open source software (Blaauw and
1486 Christen, 2011) considering the Marine curve ^{13}C (Reimer et al., 2013).

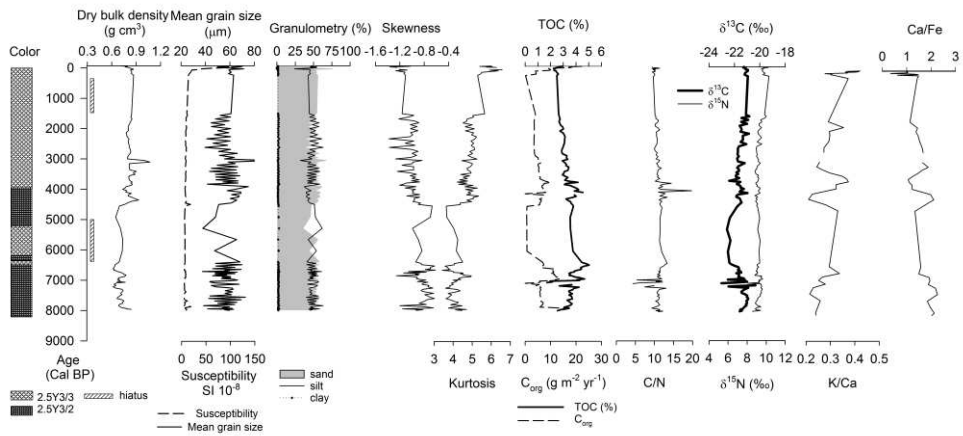


1487
1488
1489
1490
1491
1492
1493
1494
1495
1496
1497
1498

1499 Figure 5. Characterization of sediment cores retrieved from (a) Guanaqueros Bay
 1500 (BGGC5) and (b) Tongoy Bay (BTGC8), where the color (Munsell chart scale)
 1501 represents the depth, dry bulk density, mean grain size, granulometry (% sand, silt,
 1502 and clay), statistical parameters (skewness, kurtosis), organic components (TOC, C/N ratio,
 1503 stable isotopes $\delta^{15}\text{N}$ and $\delta^{13}\text{C}$) and chemical composition (K/Ca, Ca/Fe).

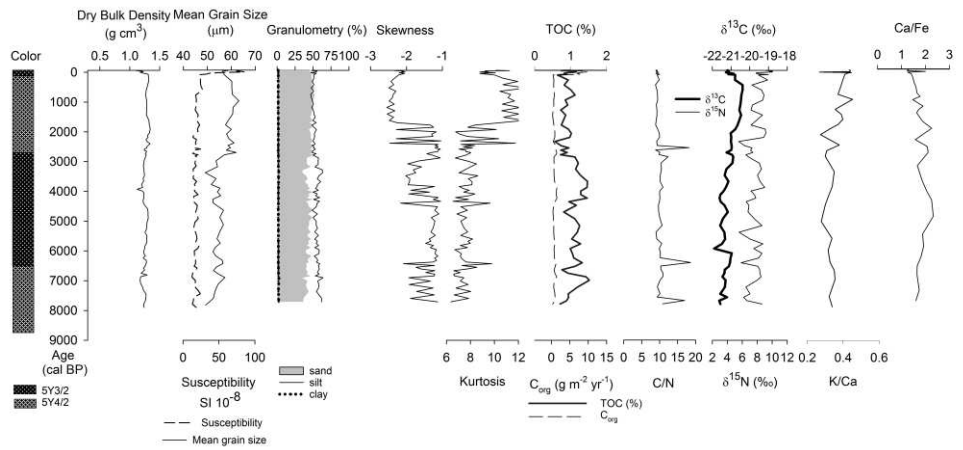
1504

1505 a)



1506

1507 b)



1508

1509

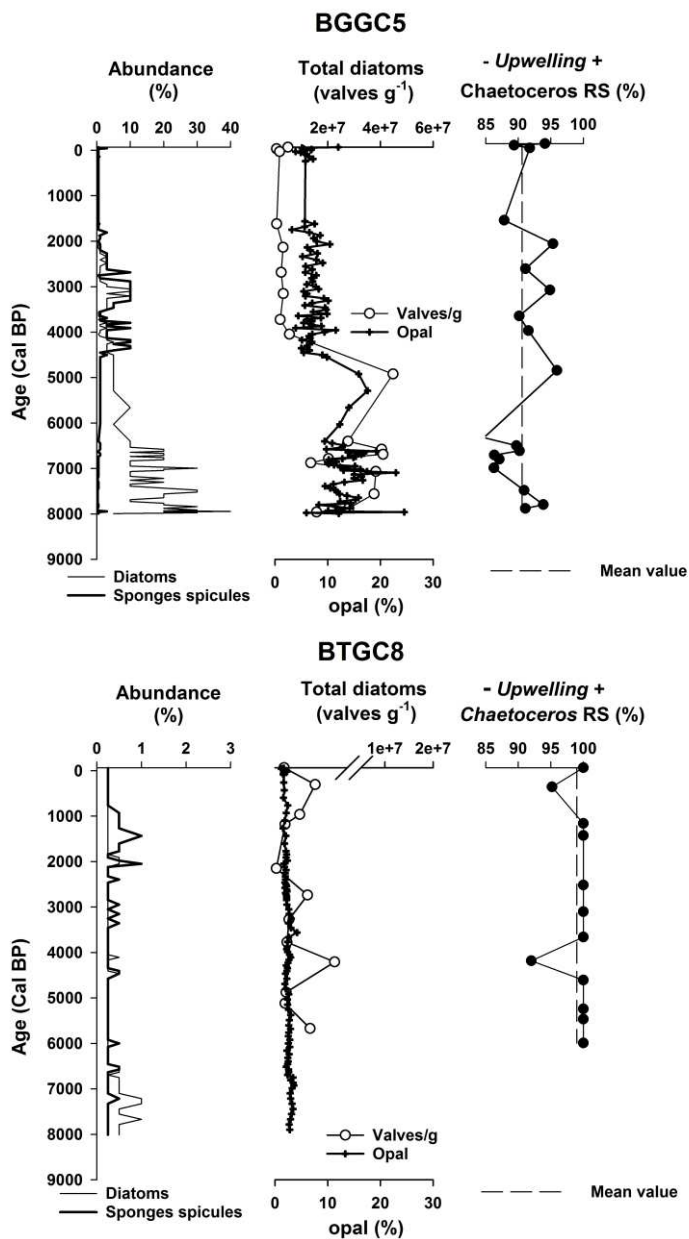
1510

1511

1512

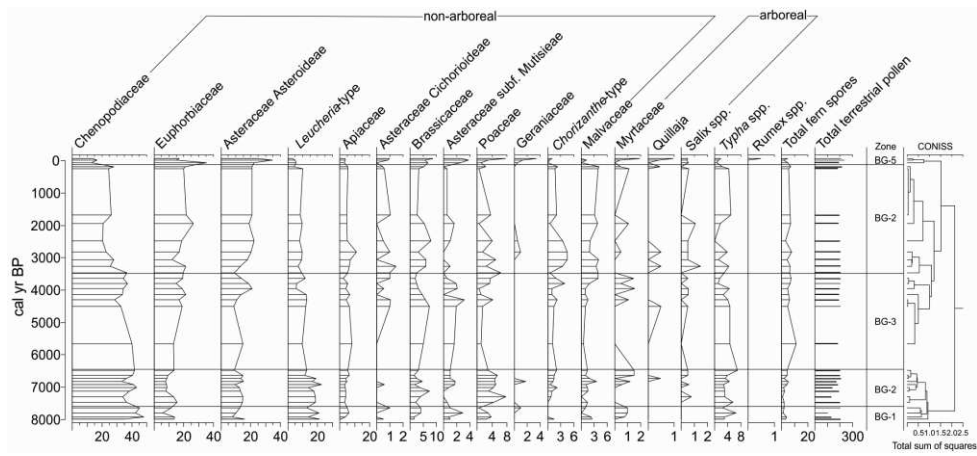
1513

1514 Figure 6. Diatom and sponge spicule relative abundances, total diatom counts (valves g^{-1}) and opal (%), and downcore variations in *Ch.* RS percentages as proxies of upwelling
 1515 intensity in the BGGC5 and BTGC8 cores (Guanaqueros and Tongoy Bay,
 1516 respectively). The medium dashed line represents the average of *Ch. resting* spores for
 1517 the respective core.
 1518
 1519



1520
 1521

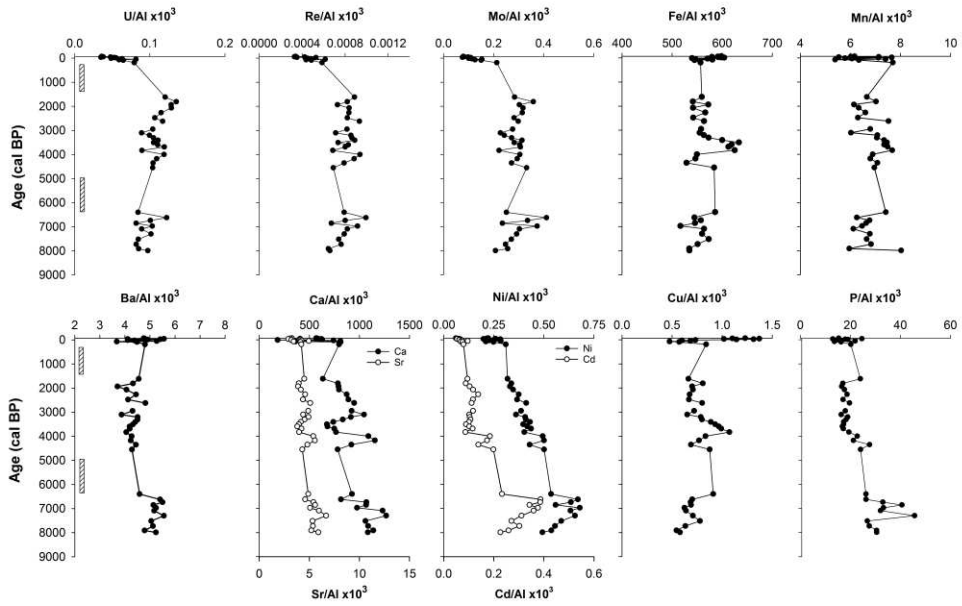
1522 Figure 7. Pollen record in BGGC5 core.



- 1523
- 1524
- 1525
- 1526
- 1527
- 1528
- 1529
- 1530
- 1531
- 1532
- 1533
- 1534
- 1535
- 1536
- 1537
- 1538
- 1539
- 1540
- 1541
- 1542
- 1543
- 1544
- 1545

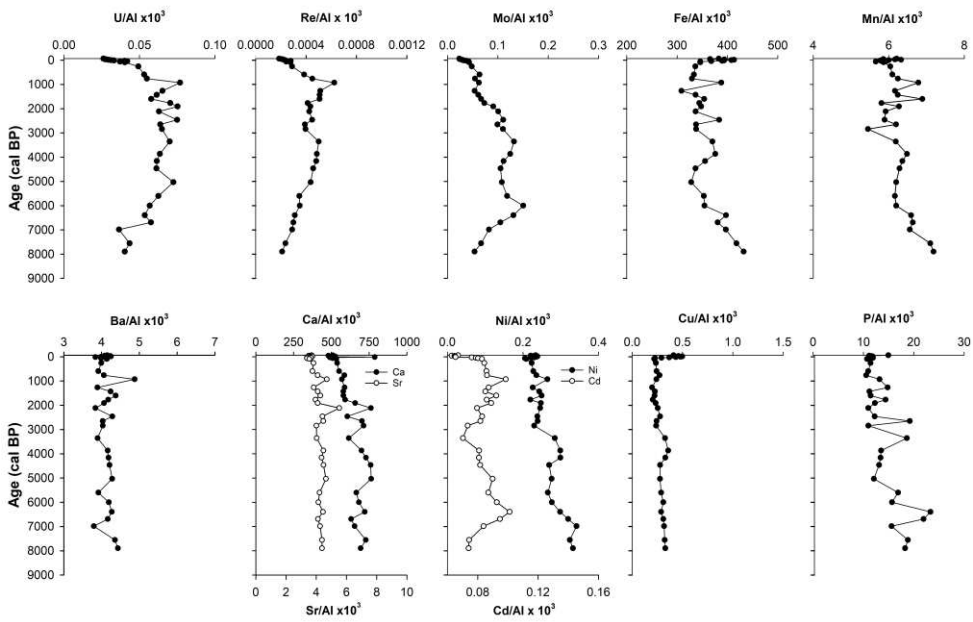
1546 Figure 8. Downcore trace element variations in: (a) Guanaqueros Bay (BGGC5) and (b)
 1547 Tongoy Bay (BTGC8), off Coquimbo (30 °S).

1548 a)



1549

1550 b)



1551

1552

1553 Figure 9. Opal accumulation and authigenic enrichment factor (EF) of trace elements
 1554 calculated for Guanaqueros Bay (BGGC5 core). Lithogenic background was estimated
 1555 from the surface sediments of Pachingo wetland cores (see text). Pollen moisture index
 1556 defined as the normalized ratio between Euphorbiaceae (wet coastal shrub land) and
 1557 Chenopodiaceae (arid scrubland). Positive (negative) values for this index indicate the
 1558 relative expansion (reduction) of coastal vegetation under wetter (drier) conditions. Pb
 1559 and Al distribution at BGGC5 core, representatives of terrigenous input to the bay.
 1560

